

Precoder Design and Statistical Power Allocation for MIMO-NOMA via User-Assisted Simultaneous Diagonalization

Aravindh Krishnamoorthy,^{*†} Zhiguo Ding,[‡] and Robert Schober^{*}

^{*}Friedrich-Alexander-Universität Erlangen-Nürnberg, [†]Fraunhofer Institute for Integrated Circuits (IIS),

[‡]The University of Manchester

Abstract

In this paper, we investigate the downlink precoder design for two-user power-domain multiple-input multiple-output (MIMO) non-orthogonal multiple access (NOMA). We propose a novel user-assisted (UA) simultaneous diagonalization (SD) based MIMO-NOMA scheme that achieves SD of the MIMO channels of both users through a combination of precoder design and low-complexity self-interference cancellation at the users, thereby considerably lowering the overall decoding complexity compared to joint decoding. The achievable ergodic user rates of the proposed scheme are analyzed for Rayleigh fading channels based on a finite-size random matrix theory framework, which is further exploited to develop a statistical power allocation algorithm. Simulation and numerical results show that the proposed UA-SD MIMO-NOMA scheme significantly outperforms orthogonal multiple access and a benchmark precoder design performing SD via generalized singular value decomposition in terms of the achievable ergodic rate region for most user rates. The ergodic rate region is further enhanced by a hybrid scheme which performs time sharing between the proposed UA-SD MIMO-NOMA scheme and single-user MIMO.

I. INTRODUCTION

Non-orthogonal multiple access (NOMA), proposed in [3], aims to improve the downlink spectral efficiency and user fairness of wireless communication systems, by exploiting superposition coding at the transmitter and successive interference cancellation (SIC) at the receivers, compared to orthogonal multiple access (OMA) [4], [5]. Although the authors of [3] primarily

This paper was presented in part at the IEEE Int. Conf. Commun. (ICC) 2019 [1] and the 24th Intl. ITG Workshop on Smart Antennas [2]. Computer programs for the most important analytical results in this paper can be downloaded from <https://gitlab.com/aravindh.krishnamoorthy/mimo-noma>.

considered NOMA employing power-domain superposition coding, other forms of NOMA based on code division multiple access (CDMA) have been proposed as well [4]–[6]. Nevertheless, in this paper, we focus on power-domain NOMA owing to its simplicity and compatibility with the existing 4th generation (4G) networks.

While most of the early works on NOMA considered single-antenna transmitters [3], [7], the extension of NOMA to multiple-input multiple-output (MIMO) systems is of interest as it has the potential of combining the benefits of the multiple spatial streams facilitated by MIMO with the increased spectral efficiency and user fairness enabled by NOMA. Various works have shown that power-domain MIMO-NOMA enables significantly higher data rates compared to MIMO-OMA [8], [9]. However, a careful MIMO precoder design was found to be crucial for realizing the potential performance gains [10]. To this end, multiple MIMO-NOMA precoder designs have been reported. In particular, a model for quasi-degradation was proposed for multiple-input single-output (MISO) channels in [11], [12], and exploited for the development of a precoder for MISO channels. Extensions to MIMO channels were reported in [10], [13], [14] based on user signal alignment. Optimal power allocation to further improve the performance of various precoding schemes was considered in [15]–[20].

However, most existing precoding schemes entail a high decoding complexity at the receivers owing to the need for self- and inter-user-interference cancellation. In order to reduce the decoding complexity at the users, the authors of [21], [22] proposed a two-user MIMO-NOMA scheme employing simultaneous diagonalization (SD) of the MIMO channels of the users via generalized singular value decomposition (GSVD). The resulting precoding scheme decomposes the MIMO-NOMA channels of the users into multiple single-input single-output (SISO)-NOMA channels, thereby enabling low-complexity decoding. In addition, the authors of [22] analyzed the achievable ergodic user rates of GSVD-based precoding for asymptotically large numbers of antennas via random matrix theory (RMT) for Rayleigh fading channels with equal power allocation (EPA).

Although GSVD-based precoding enables SD, it also suffers from several shortcomings. Importantly, GSVD-based precoding has poor performance if the sum of the numbers of receiver antennas approaches the number of antennas at the base station (BS). Furthermore, GSVD requires the inversion of the MIMO channels of both users, which also degrades performance.

In this paper, we propose a novel user-assisted (UA)-SD MIMO-NOMA scheme that simultaneously diagonalizes the MIMO channels of both users through a combination of precoder design

and low-complexity self-interference cancellation at the users, and overcomes the shortcomings of GSVD-based precoding. Furthermore, we develop a finite-size RMT based framework in order to analyze the achievable ergodic rate of the proposed MIMO-NOMA precoding scheme in Rayleigh fading for a finite number of antennas, where both EPA and unequal power allocation (UPA) are considered. Moreover, we present large finite-dimension approximations for the achievable ergodic rate.

This paper builds upon the conference versions in [1] and [2], which introduced UA-SD MIMO-NOMA for the case where the number of receiver antennas is less than the number of BS antennas, and EPA with fixed [1] and flexible [2] partitioning of the power between the users. In this paper, we generalize the proposed MIMO-NOMA scheme to all possible antenna configurations and UPA. Furthermore, we extend the analysis and simulation results, and provide proofs for the derived analytical results. The main contributions of this paper can be summarized as follows.

- We propose downlink two-user power-domain UA-SD MIMO-NOMA precoding and decoding schemes which decompose the MIMO-NOMA channels of the users into multiple SISO-NOMA channels, assuming low-complexity self-interference cancellation at one of the users.
- We develop a finite-size RMT framework to evaluate the achievable ergodic user rates of the proposed MIMO-NOMA scheme in Rayleigh fading for EPA and UPA, respectively. Furthermore, we develop a long-term power allocation scheme requiring knowledge of only the channel statistics.
- Lastly, we exploit the developed finite-size RMT framework to obtain the ergodic achievable rate region of the proposed MIMO-NOMA scheme. A comparison with GSVD-based precoding and OMA reveals significant performance gains for most user rates.

The remainder of this paper is organized as follows. In Section II, we present the MIMO-NOMA system model and briefly review the existing SD schemes. In Section III, we present the proposed UA-SD MIMO-NOMA precoding and decoding schemes. In Section IV, we develop finite-size RMT based analysis frameworks for EPA and UPA, respectively, and a statistical power allocation algorithm. In Section V, we present the simulation results, and Section VI concludes the paper.

Notation: Boldface capital letters \mathbf{X} and lower case letters \mathbf{x} denote matrices and vectors, respectively. \mathbf{X}^T , \mathbf{X}^H , \mathbf{X}^+ , $\mathbf{X}^{\frac{1}{2}}$, $\text{tr}(\mathbf{X})$, and $\det(\mathbf{X})$ denote the transpose, Hermitian transpose, respectively.

Moore-Penrose pseudoinverse, symmetric square root, trace, and determinant of matrix \mathbf{X} , respectively. Furthermore, $\text{col}(\mathbf{X})$ and $\text{null}(\mathbf{X})$ denote the column space and null space of matrix \mathbf{X} , respectively. $\mathbb{C}^{m \times n}$ and $\mathbb{R}^{m \times n}$ denote the set of all $m \times n$ matrices with complex-valued and real-valued entries, respectively. The (i, j) -th entry of a matrix \mathbf{X} is denoted by $[\mathbf{X}]_{ij}$. Moreover, $\text{diag}(d_1, \dots, d_n)$ denotes a diagonal matrix with diagonal elements $\{d_1, \dots, d_n\}$. \mathbf{I}_n denotes the $n \times n$ identity matrix, and $\mathbf{0}$ denotes an all-zeros matrix of appropriate dimension. The circularly symmetric complex Gaussian (CSCG) distribution with mean $\boldsymbol{\mu}$ and covariance matrix $\boldsymbol{\Sigma}$ is denoted by $\mathcal{CN}(\boldsymbol{\mu}, \boldsymbol{\Sigma})$ and the matrix-variate Wishart distribution with parameters p and q and covariance matrix $\boldsymbol{\Sigma}$ is denoted by $\mathcal{CW}_p(q, \boldsymbol{\Sigma})$ [23, Def. 3.2.1]. \sim stands for “distributed as”. $\mathbb{E}[\cdot]$ denotes statistical expectation, and $\mathbb{1}_{\{P\}}$ denotes the indicator function with $\mathbb{1}_{\{P\}} = 1$ when the predicate P is true and 0 otherwise. For a tuple \mathbf{t} containing 2-tuples as elements, i.e., $\mathbf{t} = ((x_1, y_1), (x_2, y_2), \dots, (x_n, y_n))$, $\pi_1(\mathbf{t}) = (x_1, x_2, \dots, x_n)$ denotes the first projection, and $\pi_2(\mathbf{t}) = (y_1, y_2, \dots, y_n)$ denotes the second projection.

II. PRELIMINARIES

In this section, we present the downlink two-user MIMO-NOMA system model and briefly review existing MIMO-NOMA schemes employing SD.

A. System Model

We consider a two-user¹ downlink transmission, where the BS is equipped with N antennas, and the users have M_1 and M_2 antennas, respectively. Furthermore, we assume that user 1 is located farther away from the BS and experiences a higher path loss compared to user 2.

The MIMO channel matrix between the BS and user k , $\mathbf{H}_k, k = 1, 2$, is modeled as

$$\frac{1}{\sqrt{\Pi_k}} \mathbf{H}_k, \quad (1)$$

where matrix $\mathbf{H}_k \in \mathbb{C}^{M_k \times N}$ captures the small-scale fading effects, and its elements $[\mathbf{H}_k]_{ij} \sim \mathcal{CN}(0, 1), i = 1, \dots, M_k, j = 1, \dots, N, k = 1, 2$, are statistically independent for all i, j, k .

¹We restrict the number of paired users to two for tractability and to limit the overall decoding complexity at the receivers as pairing $K > 1$ users necessitates $K(K-1)/2$ successive interference cancellation stages. For $K > 2$ users, a hybrid approach, such as in [22, Sec. V-B], can be employed where the users are divided into groups of two users and each group is allocated orthogonal resources. Within each two-user group, the proposed MIMO-NOMA scheme can be applied.

Hence, matrices $\mathbf{H}_k, k = 1, 2$, have full column or row rank with probability one. The scalar $\Pi_k > 0, k = 1, 2$, models the path loss between the BS and user k , where $\Pi_1 > \Pi_2$.

Next, let $L = \min \{M_1 + M_2, N\}$ denote the symbol vector length, and let $\mathbf{s}_1 = [s_{1,1}, \dots, s_{1,L}]^T \in \mathbb{C}^{L \times 1}$ and $\mathbf{s}_2 = [s_{2,1}, \dots, s_{2,L}]^T \in \mathbb{C}^{L \times 1}$ denote the symbol vectors intended for the first and the second users, respectively. We assume that the $s_{k,l} \sim \mathcal{CN}(0, 1), k = 1, 2, l = 1, \dots, L$, are statistically independent for all k, l . We construct the MIMO-NOMA symbol vector $\mathbf{s} = [s_1, \dots, s_L]^T$ as follows:

$$\mathbf{s} = \text{diag}(\sqrt{p_{1,1}}, \dots, \sqrt{p_{1,L}}) \mathbf{s}_1 + \text{diag}(\sqrt{p_{2,1}}, \dots, \sqrt{p_{2,L}}) \mathbf{s}_2, \quad (2)$$

where $\mathbb{E}[\mathbf{s}_1 \mathbf{s}_1^H] = \mathbb{E}[\mathbf{s}_2 \mathbf{s}_2^H] = \mathbf{I}_L$, and $p_{k,l} \geq 0, k = 1, 2, l = 1, \dots, L$, is the transmit power allocated to the l -th symbol of user k . The MIMO-NOMA symbol vector is precoded using a linear precoder matrix $\mathbf{P} \in \mathbb{C}^{N \times L}$, resulting in the transmit signal $\mathbf{x} = \mathbf{P}\mathbf{s}$. The corresponding average transmit power, P_T , is given by

$$P_T = \mathbb{E} \left[\text{tr} \left(\mathbf{P} \text{diag}(p_{1,1} + p_{2,1}, \dots, p_{1,L} + p_{2,L}) \mathbf{P}^H \right) \right]. \quad (3)$$

At user $k, k = 1, 2$, the received signal, $\hat{\mathbf{y}}_k \in \mathbb{C}^{M_k \times 1}$, is given by

$$\hat{\mathbf{y}}_k = \frac{1}{\sqrt{\Pi_k}} \mathbf{H}_k \mathbf{x} + \hat{\mathbf{z}}_k = \frac{1}{\sqrt{\Pi_k}} \mathbf{H}_k \mathbf{P} \mathbf{s} + \hat{\mathbf{z}}_k, \quad (4)$$

where $\hat{\mathbf{z}}_k \sim \mathcal{CN}(\mathbf{0}, \sigma^2 \mathbf{I}_{M_k})$ denotes the additive white Gaussian noise (AWGN) vector. Furthermore, at user k , $\hat{\mathbf{y}}_k$ is processed by a unitary detection matrix $\mathbf{Q}_k \in \mathbb{C}^{M_k \times M_k}$ leading to

$$\mathbf{y}_k = \mathbf{Q}_k \hat{\mathbf{y}}_k = \frac{1}{\sqrt{\Pi_k}} \mathbf{Q}_k \mathbf{H}_k \mathbf{P} \mathbf{s} + \mathbf{z}_k, \quad (5)$$

where $\mathbf{z}_k = \mathbf{Q}_k \hat{\mathbf{z}}_k \sim \mathcal{CN}(\mathbf{0}, \sigma^2 \mathbf{I}_{M_k})$. \mathbf{y}_k is subsequently used for detection.

B. Existing Simultaneous Diagonalization Schemes

In this section, we briefly review the existing SD MIMO-NOMA precoding schemes based on joint zero forcing (JZF) [24], block diagonalization (BD) [25], and GSVD [22]. Furthermore, exploiting finite-size RMT, we derive a simplified expression for the average BS transmit power in (3) for GSVD based MIMO-NOMA, and use this result to illustrate some of the shortcomings of this precoding scheme.

1) *JZF Based Precoding [24]*: SD of the MIMO channels of the users can be accomplished via JZF if sufficient degrees of freedom (DoFs) are available at the BS, i.e., if $M_1 + M_2 \leq N$. In this case, from [24], the precoding and detection matrices are given by $\mathbf{Q}_1 = \mathbf{I}_{M_1}$, $\mathbf{Q}_2 = \mathbf{I}_{M_2}$, and $\mathbf{P} = \mathbf{H}^+$, where $\mathbf{H} = \begin{bmatrix} \mathbf{H}_1^T & \mathbf{H}_2^T \end{bmatrix}^T$. Using the above precoder and detection matrices, $\mathbf{Q}_1 \mathbf{H}_1 \mathbf{P} = \begin{bmatrix} \mathbf{I}_{M_1} & \mathbf{0} \end{bmatrix}$ and $\mathbf{Q}_2 \mathbf{H}_2 \mathbf{P} = \begin{bmatrix} \mathbf{0} & \mathbf{I}_{M_2} \end{bmatrix}$.

2) *BD Based Precoding [25]*: SD of the MIMO channels of the users can be performed based on BD if sufficient DoFs are available at the BS, i.e., if $M_1 + M_2 \leq N$. Let a basis of null(\mathbf{H}_1) and null(\mathbf{H}_2) be contained in $\bar{\mathbf{H}}_1 \in \mathbb{C}^{L \times M_2}$ and $\bar{\mathbf{H}}_2 \in \mathbb{C}^{L \times M_1}$ with dimensions² M_2 and M_1 , respectively. For BD, from [25], the precoding and detection matrices are given by $\mathbf{Q}_1 = \mathbf{U}_1^H$, $\mathbf{Q}_2 = \mathbf{U}_2^H$, and $\mathbf{P} = \begin{bmatrix} \frac{1}{\sqrt{M_1}} \bar{\mathbf{H}}_2 \mathbf{V}_1 & \frac{1}{\sqrt{M_2}} \bar{\mathbf{H}}_1 \mathbf{V}_2 \end{bmatrix}$, where $\mathbf{U}_1 \in \mathbb{C}^{M_1 \times M_1}$, $\mathbf{U}_2 \in \mathbb{C}^{M_2 \times M_2}$, $\mathbf{V}_1 \in \mathbb{C}^{N \times M_1}$, and $\mathbf{V}_2 \in \mathbb{C}^{N \times M_2}$ are unitary matrices obtained from the SVDs $\frac{1}{\sqrt{M_1}} \mathbf{H}_1 \bar{\mathbf{H}}_2 = \mathbf{U}_1 \Sigma_1 \mathbf{V}_1$ and $\frac{1}{\sqrt{M_2}} \mathbf{H}_2 \bar{\mathbf{H}}_1 = \mathbf{U}_2 \Sigma_2 \mathbf{V}_2$, and Σ_1 and Σ_2 contain the singular values of $\frac{1}{\sqrt{M_1}} \mathbf{H}_1 \bar{\mathbf{H}}_2$ and $\frac{1}{\sqrt{M_2}} \mathbf{H}_2 \bar{\mathbf{H}}_1$ on their main diagonals, respectively. Furthermore, as $\bar{\mathbf{H}}_2 \mathbf{V}_1$ and $\bar{\mathbf{H}}_1 \mathbf{V}_2$ are unitary matrices, (3) simplifies to

$$P_T = \sum_{k=1}^2 \frac{1}{M_k} \sum_{l=1}^L p_{k,l}. \quad (6)$$

Using the above precoder and detection matrices, we have $\mathbf{Q}_1 \mathbf{H}_1 \mathbf{P} = \Sigma_1$ and $\mathbf{Q}_2 \mathbf{H}_2 \mathbf{P} = \Sigma_2$.

The JZF and BD based precoding schemes may be interpreted as special cases of MIMO-NOMA, where no symbols are simultaneously transmitted to both users, and are equivalent to spatial OMA. Next, we review GSVD-based precoding which can simultaneously diagonalize the MIMO channels of the users also for $M_1 + M_2 > N$.

3) *GSVD Based Precoding [21], [22]*: GSVD [26], [27] is a matrix decomposition technique that simultaneously diagonalizes two matrices having equal numbers of columns. For the problem at hand, channel matrices \mathbf{H}_1 and \mathbf{H}_2 may be simultaneously diagonalized as follows:

$$\mathbf{Q}_1 \mathbf{H}_1 \mathbf{Z} = \mathbf{C}, \quad \mathbf{Q}_2 \mathbf{H}_2 \mathbf{Z} = \mathbf{S}, \quad (7)$$

where $\mathbf{Z} \in \mathbb{C}^{N \times L}$ is a full matrix, $\mathbf{C} \in \mathbb{R}^{M_1 \times L}$ and $\mathbf{S} \in \mathbb{R}^{M_2 \times L}$ are given by

$$\mathbf{C} = \begin{bmatrix} \mathbf{0} & \mathbf{C}_1 & \mathbf{0} \\ \mathbf{0} & \mathbf{0} & \mathbf{I}_{\bar{M}_1} \end{bmatrix}, \quad \mathbf{S} = \begin{bmatrix} \mathbf{I}_{\bar{M}_2} & \mathbf{0} & \mathbf{0} \\ \mathbf{0} & \mathbf{S}_1 & \mathbf{0} \end{bmatrix}, \quad (8)$$

such that $\mathbf{C}^H \mathbf{C} + \mathbf{S}^H \mathbf{S} = \mathbf{I}_L$, and $\mathbf{Q}_1 \in \mathbb{C}^{M_1 \times M_1}$ and $\mathbf{Q}_2 \in \mathbb{C}^{M_2 \times M_2}$ are unitary matrices. Furthermore, $\bar{M}_1 = \min \{M_1, \max \{0, N - M_2\}\}$, $\bar{M}_2 = \min \{M_2, \max \{0, N - M_1\}\}$, and

²For $M_1 + M_2 \leq N$, bases $\bar{\mathbf{H}}_1$ and $\bar{\mathbf{H}}_2$ with dimensions M_2 and M_1 , respectively, can always be found.

$M = N - \bar{M}_1 - \bar{M}_2$. Moreover, $\mathbf{C}_1 \in \mathbb{R}^{M \times M}$ and $\mathbf{S}_1 \in \mathbb{R}^{M \times M}$ are diagonal matrices such that $\mathbf{C}_1 \mathbf{S}_1^{-1}$ contains the generalized singular values (GSVs) of \mathbf{H}_1 and \mathbf{H}_2 on its main diagonal.

Hence, by choosing the precoder matrix as $\mathbf{P} = \mathbf{Z}$ and the detection matrices for users 1 and 2 as \mathbf{Q}_1 and \mathbf{Q}_2 , respectively, from (7), the MIMO-NOMA channels of both users are simultaneously diagonalized into SISO-NOMA channels [22] with \mathbf{C} and \mathbf{S} as the equivalent MIMO channels for users 1 and 2, respectively.

We use GSVD-based precoding as a baseline for comparison with the proposed scheme. GSVD-based precoding [22] uses identical powers for all $s_l, l = 1, \dots, L$, i.e., $p_{1,l} + p_{2,l} = P, P \geq 0, \forall l$. Hence, in this case, (3) simplifies to the expression given in Proposition 1 below.

Proposition 1. *For GSVD-based precoding [22], (3) simplifies as follows:*

$$P_T = PL \left| \frac{1}{M_1 + M_2 - N} \right|. \quad (9)$$

Proof. Please refer to Appendix A.1. □

Remark 1. The expression given in Proposition 1 simplifies to [22, Thm. 2] for the asymptotic case $\frac{M_1}{N} = \frac{M_2}{N} = \eta, M_1, M_2, N \rightarrow \infty$.

The right hand side of (9) increases unboundedly as $M_1 + M_2 \rightarrow N$, leading to an exceedingly large transmit power. Furthermore, when $M_1 + M_2 = N$, the transmit power becomes infinite, rendering communication impossible. Moreover, from (8), the effective channels of \bar{M}_1 spatial streams of user 1 and \bar{M}_2 spatial streams of user 2 are forced to $\mathbf{I}_{\bar{M}_1}$ and $\mathbf{I}_{\bar{M}_2}$, respectively, cf. (7), (8), thereby necessitating channel inversion at the BS, which has a detrimental effect on performance. Hence, in the following, we develop the proposed UA-SD MIMO-NOMA scheme which overcomes the above limitations while still achieving SD of the users' channels.

III. THE PROPOSED UA-SD MIMO-NOMA SCHEME

In this section, we begin by describing a new matrix decomposition technique. Then, we utilize this matrix decomposition to develop the proposed UA-SD MIMO-NOMA precoding and decoding schemes. Lastly, we derive expressions for the achievable rates of the users.

A. Simultaneous Diagonalization

Let \bar{M}_1, \bar{M}_2 , and M be as defined in Section II-B3. The proposed SD matrix decomposition is compactly stated in the following theorem.

Theorem 1. Let \mathbf{H}_1 and \mathbf{H}_2 be defined as in Section II-A. Then, there exist unitary matrices $\mathbf{Q}_1 \in \mathbb{C}^{M_1 \times M_1}$ and $\mathbf{Q}_2 \in \mathbb{C}^{M_2 \times M_2}$, and a full matrix $\mathbf{Z} \in \mathbb{C}^{N \times L}$ such that

$$\mathbf{Q}_1 \mathbf{H}_1 \mathbf{Z} = \begin{bmatrix} \boldsymbol{\Sigma}_1 & \mathbf{0} & \mathbf{0} \\ \mathbf{0} & \mathbf{D}_1 & \mathbf{0} \end{bmatrix}, \quad \mathbf{Q}_2 \mathbf{H}_2 \mathbf{Z} = \begin{bmatrix} \mathbf{T} & \mathbf{0} & \mathbf{D}_2 \\ \boldsymbol{\Sigma}_2 & \mathbf{0} & \mathbf{0} \end{bmatrix}, \quad (10)$$

where $\boldsymbol{\Sigma}_1, \boldsymbol{\Sigma}_2 \in \mathbb{R}^{M \times M}$ are diagonal matrices such that $\boldsymbol{\Sigma}_2 \boldsymbol{\Sigma}_1^{-1}$ contains the GSVs of \mathbf{H}_2 and \mathbf{H}_1 on its main diagonal³, $\mathbf{T} \in \mathbb{C}^{\bar{M}_2 \times M}$ is a full matrix, and $\mathbf{D}_k \in \mathbb{R}^{\bar{M}_k \times \bar{M}_k}, k = 1, 2$, are diagonal matrices. \mathbf{D}_1 is defined as

$$\mathbf{D}_1 = \begin{cases} \mathbf{S}_1 & \text{if } M_1 + M_2 \leq N \\ \mathbf{I}_{\bar{M}_1} & \text{otherwise,} \end{cases} \quad (11)$$

where \mathbf{S}_1 contains the \bar{M}_1 singular values of $\frac{1}{\sqrt{M_1}} \mathbf{H}_1 \bar{\mathbf{H}}_2$ on its main diagonal. \mathbf{D}_2 contains the \bar{M}_2 singular values of $\frac{1}{\sqrt{M_2}} \mathbf{H}_2 \bar{\mathbf{H}}_1$ on its main diagonal.

Proof. Please refer to Appendix A.2. □

In the following, we utilize the matrix decomposition in Theorem 1 to develop the proposed precoder and decoder designs.

B. Precoder Design

Matrices \mathbf{Q}_1 and \mathbf{Q}_2 from (10) are used as detection matrices and the precoder matrix is chosen as $\mathbf{P} = \mathbf{Z}$. Hence, based on Theorem 1, the received signals at the users can be obtained from (5) as follows

$$\mathbf{y}_1 = \frac{1}{\sqrt{\Pi_1}} \begin{bmatrix} \boldsymbol{\Sigma}_1 & \mathbf{0} & \mathbf{0} \\ \mathbf{0} & \mathbf{D}_1 & \mathbf{0} \end{bmatrix} \mathbf{s} + \mathbf{z}_1, \quad (12)$$

$$\mathbf{y}_2 = \frac{1}{\sqrt{\Pi_2}} \begin{bmatrix} \mathbf{T} & \mathbf{0} & \mathbf{D}_2 \\ \boldsymbol{\Sigma}_2 & \mathbf{0} & \mathbf{0} \end{bmatrix} \mathbf{s} + \mathbf{z}_2, \quad (13)$$

where the effective channel matrix of user 1 is diagonalized and the effective channel matrix of user 2 is partially diagonalized except for matrix \mathbf{T} which causes self-interference for the first \bar{M}_2 elements of \mathbf{y}_2 . Note that the computation of $\mathbf{Q}_1, \mathbf{Q}_2, \mathbf{Z}$, and \mathbf{T} is specified in Appendix A.2.

³Note that the GSVs of \mathbf{H}_2 and \mathbf{H}_1 are the solutions $\mu \geq 0$ to the equation $\det(\mathbf{H}_2^H \mathbf{H}_2 - \mu^2 \mathbf{H}_1^H \mathbf{H}_1) = 0$. They are the inverses of the GSVs of \mathbf{H}_1 and \mathbf{H}_2 , which are the solutions $\mu' \geq 0$ to $\det(\mathbf{H}_1^H \mathbf{H}_1 - \mu'^2 \mathbf{H}_2^H \mathbf{H}_2) = 0$.

As seen from (12) and (13), symbols $s_l, l = 1, \dots, M$, are received by both users. Symbols $s_l, l = M+1, \dots, M+\bar{M}_1$, are received only by user 1, hence, $p_{2,l} = 0$ for $l = M+1, \dots, M+\bar{M}_1$. Furthermore, symbols $s_l, l = M + \bar{M}_1 + 1, \dots, L$, are received only by user 2, hence, $p_{1,l} = 0$ for $l = M + \bar{M}_1 + 1, \dots, L$.

C. Decoding Scheme

At user 1, from (12), as the channel is diagonalized and $p_{2,l} = 0$ for $l = M + 1, \dots, M + \bar{M}_1$, symbols $s_{1,l}, l = M + 1, \dots, M + \bar{M}_1$, are decoded directly from the last \bar{M}_1 elements of \mathbf{y}_1 . Next, if $M > 0$, symbols $s_{1,l}, l = 1, \dots, M$, are decoded from the first M elements of \mathbf{y}_1 treating the symbols of the second user, $s_{2,l}, l = 1, \dots, M$, as interference as in SISO-NOMA [3].

At user 2, if $M > 0$, from (13), using SIC both $s_{1,l}$ and $s_{2,l}, l = 1, \dots, M$, are decoded from the last M elements of \mathbf{y}_2 as in SISO-NOMA [3]. Next, self-interference is cancelled by subtracting the reconstructed interference, $\mathbf{T}\hat{\mathbf{s}}$, from the first \bar{M}_2 elements of \mathbf{y}_2 , resulting in the self-interference-free signal

$$\tilde{\mathbf{y}}_2 = \mathbf{y}_2 - \frac{1}{\sqrt{\Pi_2}} \begin{bmatrix} \mathbf{T}\hat{\mathbf{s}} \\ \mathbf{0} \end{bmatrix} = \frac{1}{\sqrt{\Pi_2}} \begin{bmatrix} \mathbf{0} & \mathbf{0} & \mathbf{D}_2 \\ \boldsymbol{\Sigma}_2 & \mathbf{0} & \mathbf{0} \end{bmatrix} \mathbf{s} + \mathbf{z}_2, \quad (14)$$

where the elements of $\hat{\mathbf{s}} \in \mathbb{C}^{M \times 1}$ are the previously decoded symbols⁴ $s_l = p_{1,l}s_{1,l} + p_{2,l}s_{2,l}, l = 1, \dots, M$. Lastly, symbols $s_{2,l}, l = M + \bar{M}_1 + 1, \dots, L$, are decoded from the first \bar{M}_2 elements of $\tilde{\mathbf{y}}_2$, which are interference free as $p_{1,l} = 0$ for $l = M + \bar{M}_1 + 1, \dots, L$.

Remark 2. When $\bar{M}_2 > 0$, in order to eliminate the self-interference due to \mathbf{T} , both $s_{1,l}$ and $s_{2,l}, l = 1, \dots, M$, must be decoded at user 2. Therefore, SIC has to be performed at user 2 for all SISO-NOMA symbols $s_l, l = 1, \dots, M$. This is different from GSVD-based precoding in [22], where SIC is performed at user 1 or 2 depending on the values of $[\mathbf{C}_1]_u$ and $[\mathbf{S}_1]_u, u = 1, \dots, M$, given in (8). On the other hand, when $\bar{M}_2 = 0$, as there is no self-interference due to \mathbf{T} , SIC can potentially be performed at user 1 or 2 depending on the values of $[\boldsymbol{\Sigma}_1]_u$ and $[\boldsymbol{\Sigma}_2]_u, u = 1, \dots, M$, similar to GSVD-based MIMO-NOMA. Nevertheless, we show in Section IV-A that, for the proposed scheme, the performance gain obtained by allowing flexible SIC at user 1 or 2 is insignificant when the users are located sufficiently far apart, which is the most relevant scenario for MIMO-NOMA.

⁴It is assumed that the previously decoded symbols are correctly decoded as symbols $s_{k,l}, k = 1, 2, l = 1, \dots, M$, are transmitted at or below the achievable rate $R_{k,l}$ given later in Section III-E.

TABLE I: Required operations for decomposition in Theorem 1, see Appendix A.2 for definition of matrices.

	Computation	Dimension	Operation		Computation	Dimension	Operation
1)	$\bar{\mathbf{H}}_1$	$N \times M_1$	QR decomposition	4)	$\hat{\mathbf{U}}_1 \mathbf{\Sigma}_1 \hat{\mathbf{V}}_1^H$	$M_1 \times N$	SVD
2)	$\bar{\mathbf{H}}_2$	$N \times M_2$	QR decomposition	5)	$\tilde{\mathbf{H}}_2^H = \mathbf{Q}\mathbf{R}$	$M_1 \times M_2$	QR decomposition
3)	\mathbf{K}	$N \times (\bar{M}_1 + \bar{M}_2)$	QR decomposition	6)	$\mathbf{\Sigma}$	$M \times M$	SVD

Next, we calculate the computational complexity of the proposed UA-SD MIMO-NOMA and compare it with that of GSVD-based MIMO-NOMA [22].

D. Computational Complexity

For the proposed scheme, the required operations for the matrix decomposition in Theorem 1, based on Appendix A.2, are summarized in Table I. As the QR decomposition and SVD of an $M \times N$ matrix entail complexities of $\mathcal{O}\left(2N^2(M - \frac{N}{3}) + 4(M^2N - MN^2 + \frac{N^3}{3})\right)$ and $\mathcal{O}(4M^2N + 8MN^2 + 9N^3)$, respectively [28, Sec. 5.5], obtaining $\mathbf{Q}_1, \mathbf{Q}_2$, and \mathbf{Z} based on Theorem 1 entails a total complexity of $\mathcal{O}\left(\frac{134}{3}N^3\right)$ for $M_1 = M_2 = N$. Furthermore, in the proposed scheme, self-interference cancellation at user 2 entails an additional complexity of $\mathcal{O}(M\bar{M}_2)$. On the other hand, GSVD used in [22] requires a QR decomposition of size $(M_1 + M_2) \times N$ and a cosine-sine (CS) decomposition [29] of size $M_1 + M_2$. The CS decomposition entails a complexity of $\mathcal{O}(36N^3)$, resulting in an overall complexity of $\mathcal{O}\left(\frac{116}{3}N^3\right)$ for $M_1 = M_2 = N$. Hence, both the proposed UA-SD MIMO-NOMA and GSVD-based MIMO-NOMA [22] have an overall complexity order of $\mathcal{O}(N^3)$.

E. Achievable Rates

Based on (12), the achievable rates for the $s_{1,l}, l = 1, \dots, L$, of user 1 are given by

$$R_{1,l}^{(1)} = \begin{cases} \log_2 \left(1 + \frac{p_{1,l}}{\Pi_1} \frac{([\mathbf{\Sigma}_1]_l)^2}{\sigma^2 + \frac{p_{2,l}}{\Pi_1} ([\mathbf{\Sigma}_1]_l)^2} \right) & \text{for } l = 1, \dots, M \\ \log_2 \left(1 + \frac{p_{1,l}}{\Pi_1} \frac{([\mathbf{D}_1]_l)^2}{\sigma^2} \right) & \text{for } l = M + 1, \dots, M + \bar{M}_1 \\ 0 & \text{otherwise.} \end{cases} \quad (15)$$

At user 2, in order to perform SIC, the $s_{1,l}, l = 1, \dots, M$, are decoded first. From (13), the achievable rates for the $s_{1,l}, l = 1, \dots, M$, at user 2 are given by

$$R_{1,l}^{(2)} = \log_2 \left(1 + \frac{p_{1,l}}{\Pi_2} \frac{([\mathbf{\Sigma}_2]_l)^2}{\sigma^2 + \frac{p_{2,l}}{\Pi_2} ([\mathbf{\Sigma}_2]_l)^2} \right). \quad (16)$$

For the decoding of the $s_{1,l}, l = 1, \dots, M$, to be successful at both user 1 and 2 *for every channel use*, the code rate is chosen as follows:

$$R_{1,l} = \min \left\{ R_{1,l}^{(1)}, R_{1,l}^{(2)} \right\} = \begin{cases} R_{1,l}^{(1)} & \text{if } \frac{([\Sigma_1]_{ll})^2}{\Pi_1} < \frac{([\Sigma_2]_{ll})^2}{\Pi_2} \\ R_{1,l}^{(2)} & \text{otherwise.} \end{cases} \quad (17)$$

Next, from (13) and (14), the achievable rates for the $s_{2,l}, l = 1, \dots, L$, after SIC and self-interference cancellation are given by

$$R_{2,l} = \begin{cases} \log_2 \left(1 + \frac{p_{2,l}}{\Pi_2} \frac{([\Sigma_2]_{ll})^2}{\sigma^2} \right) & \text{for } l = 1, \dots, M \\ \log_2 \left(1 + \frac{p_{2,l}}{\Pi_2} \frac{([D_2]_{ll})^2}{\sigma^2} \right) & \text{for } l = M + \bar{M}_1 + 1, \dots, L \\ 0 & \text{otherwise.} \end{cases} \quad (18)$$

Lastly, the ergodic achievable sum rates for users 1 and 2, R_1 and R_2 , respectively, are given by

$$R_1 = \mathbb{E} \left[\sum_{l=1}^M R_{1,l} \right] + \mathbb{E} \left[\sum_{l=M+1}^{M+\bar{M}_1} R_{1,l}^{(1)} \right], \quad R_2 = \mathbb{E} \left[\sum_{l=1}^M R_{2,l} \right] + \mathbb{E} \left[\sum_{l=M+\bar{M}_1+1}^L R_{2,l} \right]. \quad (19)$$

Remark 3. The diagonal entries of Σ_1 and Σ_2 contain the GSVs of \mathbf{H}_2 and \mathbf{H}_1 , c.f. Theorem 1. In [22], analogous ergodic rate expressions for GSVD-based NOMA with EPA are simplified using the asymptotic probability density function (pdf) of GSVs. However, simplification of (19) for finite M_1, M_2 , and N necessitates a novel approach based on the finite-size marginal and ordered pdfs of the GSVs, which are derived in the following section.

IV. PERFORMANCE ANALYSIS AND POWER ALLOCATION

In this section, the ergodic achievable rate expressions of the proposed UA-SD MIMO-NOMA, provided in (19), are simplified via finite-size RMT for EPA and UPA. Furthermore, a power allocation algorithm for UPA is presented.

A. Equal Power Allocation

For EPA, the same power P is allocated to all symbols $s_l, l = 1, \dots, L$. Furthermore, for $l = 1, \dots, M$, P is partitioned between users 1 and 2 as $p_{1,l} = P_1$ and $p_{2,l} = P_2$, respectively, such that $P_1 + P_2 = P$. For EPA, the transmit power in (3) can be simplified as follows.

Proposition 2. *For EPA, (3) simplifies as follows:*

$$P_T = P \left(\frac{M_1}{N} + \frac{\bar{M}_1}{M} + \mathbb{1}_{\{\bar{M}_2 > 0\}} \right), \quad (20)$$

if $M_1 + M_2 > N$, and $P_T = 2P$ otherwise.

Proof. Please refer to A.3. □

Next, we use the following definition to simplify the ergodic rate expressions of the users.

Definition 1 (Based on [30]). Let \mathbf{X} be a $q \times q$ Hermitian symmetric random matrix with eigenvalues $\lambda_1 \geq \lambda_2 \geq \dots \geq \lambda_q$, and let $\boldsymbol{\lambda} = \{\lambda_n, n = 1, \dots, q\}$. Furthermore, let the unordered eigenvalue of \mathbf{X} be denoted by $\lambda(\mathbf{X})$ and the joint pdf of the eigenvalues by $p_{\boldsymbol{\lambda}}(\boldsymbol{\lambda})$. Then, the marginal eigenvalue pdf is defined as

$$p_{\lambda(\mathbf{X})}(\lambda) = \int_0^{+\infty} \dots \int_0^{+\infty} p_{\boldsymbol{\lambda}}(\boldsymbol{\lambda}) d\lambda_q d\lambda_{q-1} \dots d\lambda_2 \Big|_{\lambda_1 \rightarrow \lambda}. \quad (21)$$

Using the above definition, for a $q \times q$ Hermitian symmetric random matrix \mathbf{X} with eigenvalues $\lambda_1, \lambda_2, \dots, \lambda_q$, we may simplify the expectation of a generic additively separable function

$$f(\lambda_1, \dots, \lambda_q) = \sum_{n=1}^q g(\lambda_n) \quad (22)$$

in the eigenvalues of \mathbf{X} as

$$\begin{aligned} \mathbb{E}[f(\lambda_1, \dots, \lambda_q)] &= \int_0^{+\infty} \dots \int_0^{+\infty} f(\lambda_1, \dots, \lambda_q) p_{\boldsymbol{\lambda}}(\boldsymbol{\lambda}) d\lambda_q \dots d\lambda_1 = \sum_{n=1}^q \int_0^{+\infty} \dots \int_0^{+\infty} g(\lambda_n) p_{\boldsymbol{\lambda}}(\boldsymbol{\lambda}) d\lambda_q \dots d\lambda_1 \\ &\stackrel{(a)}{=} q \int_0^{+\infty} g(\lambda) p_{\lambda(\mathbf{X})}(\lambda) d\lambda, \end{aligned} \quad (23)$$

where (a) is obtained by using Definition 1 and exploiting the symmetry in the integration variable. Before we can exploit (23) to calculate the ergodic rates of the users, we need to characterize the diagonal elements of $\boldsymbol{\Sigma}_1$ and $\boldsymbol{\Sigma}_2$, cf. Section III-E.

Proposition 3. When $M_1 + M_2 > N$, the squares of the l -th diagonal elements, $l = 1, \dots, M$, of matrices $\boldsymbol{\Sigma}_1$ and $\boldsymbol{\Sigma}_2$ are given by

$$[\boldsymbol{\Sigma}_1]_{ll}^2 = \frac{1}{\lambda_l + 1}, \quad [\boldsymbol{\Sigma}_2]_{ll}^2 = \frac{\lambda_l}{\lambda_l + 1}, \quad (24)$$

where λ_l is the l -th ordered eigenvalue of the F -distributed matrix $\mathbf{F} = (\mathbf{W}_2)^{\frac{1}{2}} \mathbf{W}_1^{-1} (\mathbf{W}_2)^{\frac{1}{2}}$ [31], [32], and $\mathbf{W}_2 \sim \mathcal{CW}_{\nu}(\mu_2, \mathbf{I}_{\nu})$ and $\mathbf{W}_1 \sim \mathcal{CW}_{\nu}(\mu_1, \mathbf{I}_{\nu})$ are independent Wishart distributed matrices. Coefficients μ_1, μ_2 , and ν are given in Table II.

Proof. Please refer to Appendix A.4. □

Remark 4. When $M_1 + M_2 \leq N$, as $M = 0$, matrices $\boldsymbol{\Sigma}_1$ and $\boldsymbol{\Sigma}_2$ are empty.

TABLE II: Wishart matrix parameters μ_1, μ_2, ν for different M_1, M_2 , and N .

Condition	(μ_1, μ_2, ν)	Condition	(μ_1, μ_2, ν)
$M_1, M_2 \geq N$	(M_1, M_2, N)	$M_1, M_2 < N, M_1 + M_2 > N$	(M_1, M_2, M)
$M_1 \geq N, M_2 < N$	$(M_1 + M_2 - N, N, M_2)$	$M_1 < N, M_2 \geq N$	$(N, M_1 + M_2 - N, M_1)$

Next, in Theorem 2, we present the marginal eigenvalue pdf of an \mathbf{F} distributed matrix, $p_{\lambda(\mathfrak{F})}(\lambda; \mu_1, \mu_2, \nu)$, which is then used to simplify the ergodic rates $R_{1,l}$ and $R_{2,l}$, $l = 1, \dots, M$, for EPA.

Theorem 2. Let $\mathbf{X} \sim \mathcal{CW}_q(m_1, \mathbf{I}_q)$ and $\mathbf{Y} \sim \mathcal{CW}_q(m_2, \mathbf{I}_q)$, $m_1, m_2 \geq q$, be $q \times q$ independent complex-valued Wishart random matrices. Then, the marginal eigenvalue pdf of matrix $\mathbf{F} = \mathbf{Y}^{\frac{1}{2}} \mathbf{X}^{-1} \mathbf{Y}^{\frac{1}{2}}$ is given by

$$p_{\lambda(\mathfrak{F})}(\lambda; m_1, m_2, q) = K_{\mathfrak{F}} \frac{1}{(1 + \lambda)^{m_1 + m_2}} \sum_{m=1}^q \sum_{n=1}^q (-1)^{(n+m)} \lambda^{m+n-2+m_2-q} \det(\Xi^{[m,n]}), \quad (25)$$

where $K_{\mathfrak{F}}$ is a constant ensuring that the integral over the pdf is equal to one, and the elements of the $(q-1) \times (q-1)$ matrix $\Xi^{[m,n]}$ are given by

$$[\Xi^{[m,n]}]_{ij} = B(m_2 - q + \alpha(i, j, m, n) + 1, m_1 + q - \alpha(i, j, m, n) - 1), \quad (26)$$

for $i, j = 1, \dots, q-1$, where $B(\cdot, \cdot)$ denotes the Beta function, and

$$\alpha(i, j, m, n) = \begin{cases} i + j - 2 & \text{if } i < m \text{ and } j < n \\ i + j & \text{if } i \geq m \text{ and } j \geq n \\ i + j - 1 & \text{otherwise.} \end{cases} \quad (27)$$

The support of the pdf is $\lambda \in [0, +\infty)$.

Proof. Please refer Appendix A.5. □

Remark 5. Theorem 2 is the finite-size counterpart to [22, Thm. 1]. Furthermore, the finite-size marginal eigenvalue pdf for the special case $M_1 = M_2$ has been provided in [33, Thm. 2].

Now, in order to simplify $R_{1,l}^{(1)}$, $l = M+1, \dots, M_1$, and $R_{2,l}$, $l = M_1+1, \dots, L$, we utilize the following result.

Proposition 4. The squares of the l -th diagonal elements of \mathbf{D}_1 and \mathbf{D}_2 are given by

$$([\mathbf{D}_1]_u)^2 = \begin{cases} 1 & \text{if } M_1 + M_2 > N \\ \lambda_l^{(1)} & \text{otherwise,} \end{cases}, \quad ([\mathbf{D}_2]_u)^2 = \lambda_l^{(2)}, \quad (28)$$

where $\lambda_l^{(1)}$ and $\lambda_l^{(2)}$ follow the same distributions as the l -th eigenvalues of the Wishart matrices $\mathbf{W}_1 \sim \mathcal{CW}_{\bar{M}_1}(M_1, \frac{1}{\bar{M}_1} \mathbf{I}_{\bar{M}_1})$ and $\mathbf{W}_2 \sim \mathcal{CW}_{\bar{M}_2}(M_2, \frac{1}{\bar{M}_2} \mathbf{I}_{\bar{M}_2})$, respectively.

Proof. If $M_1 + M_2 \leq N$, as the $([\mathbf{D}_1]_{ll})^2$ are the squared singular values of $\frac{1}{\sqrt{\bar{M}_1}} \mathbf{H}_1 \bar{\mathbf{H}}_2$, cf. Theorem 1, their distribution is identical to the distribution of the eigenvalues of Wishart matrix $\mathbf{W}_1 \sim \mathcal{CW}_{\bar{M}_1}(M_1, \frac{1}{\bar{M}_1} \mathbf{I}_{\bar{M}_1})$ [23, Thm. 3.2.4]. Otherwise, if $M_1 + M_2 > N$, from (11), $([\mathbf{D}_1]_{ll})^2 = 1$. Similarly, the distribution of $([\mathbf{D}_2]_{ll})^2$ is identical to the distribution of the eigenvalues of Wishart matrix $\mathbf{W}_2 \sim \mathcal{CW}_{\bar{M}_2}(M_2, \frac{1}{\bar{M}_2} \mathbf{I}_{\bar{M}_2})$. \square

The marginal eigenvalues of \mathbf{W}_1 and \mathbf{W}_2 , denoted by $p_{\lambda(\mathfrak{W})}(\lambda; M_1, \bar{M}_1)$ and $p_{\lambda(\mathfrak{W})}(\lambda; M_2, \bar{M}_2)$, respectively, can be obtained from Theorem 3.

Theorem 3. Let \mathbf{W} be a $q \times q$ complex-valued Wishart matrix $\mathbf{W} \sim \mathcal{CW}_q(p, \frac{1}{q} \mathbf{I}_q)$, $p \geq q$, then the marginal eigenvalue pdf of \mathbf{W} is given by

$$p_{\lambda(\mathfrak{W})}(\lambda; p, q) = K_{\mathfrak{W}} \sum_{m=1}^q \sum_{n=1}^q (-1)^{(n+m)} (q\lambda)^{n+m-2+p-q} \exp(-q\lambda) \det(\boldsymbol{\Omega}^{[m,n]}), \quad (29)$$

where $K_{\mathfrak{W}}$ is a constant ensuring that the integral over the pdf is equal to one, and the elements of $(q-1) \times (q-1)$ matrix $\boldsymbol{\Omega}^{[m,n]}$ are given by

$$[\boldsymbol{\Omega}^{[m,n]}]_{ij} = (\alpha(i, j, m, n) + p - q)!, \quad (30)$$

for $i, j = 1, \dots, q-1$, and $\alpha(i, j, m, n)$ is defined as in Theorem 2. The support of the pdf is $\lambda \in [0, +\infty)$.

Proof. Eq. (29) follows directly from [30, Sec. IV.A]. \square

Now, we are ready to present the ergodic user rate expressions for EPA in the following proposition.

Proposition 5. For EPA and $M_1 + M_2 \leq N$, the ergodic rates of users 1 and 2 for the proposed UA-SD MIMO-NOMA are given by

$$R_1 = \bar{M}_1 \int_0^{+\infty} \log_2 \left(1 + \frac{P\lambda}{\Pi_1 \sigma^2} \right) p_{\lambda(\mathfrak{W})}(\lambda; M_1, \bar{M}_1) d\lambda, \quad (31)$$

$$R_2 = \bar{M}_2 \int_0^{+\infty} \log_2 \left(1 + \frac{P\lambda}{\Pi_2 \sigma^2} \right) p_{\lambda(\mathfrak{W})}(\lambda; M_2, \bar{M}_2) d\lambda, \quad (32)$$

and for EPA and $M_1 + M_2 > N$, the rates are given by

$$R_1 = M \int_0^{\Pi^{-1}} \log_2 \left(1 + \frac{1}{\Pi_2 \sigma^2 + \frac{1}{\Pi_2} \frac{\lambda P_1}{1+\lambda}} \right) p_{\lambda(\mathfrak{F})}(\lambda; \mu_1, \mu_2, \nu) d\lambda$$

$$+ M \int_{\Pi^{-1}}^{+\infty} \log_2 \left(1 + \frac{1}{\Pi_1} \frac{\frac{P_1}{1+\lambda}}{\sigma^2 + \frac{1}{\Pi_1} \frac{P_2}{1+\lambda}} \right) p_{\lambda(\mathfrak{F})}(\lambda; \mu_1, \mu_2, \nu) d\lambda + \bar{M}_1 \log_2 \left(1 + \frac{P}{\Pi_1 \sigma^2} \right), \quad (33)$$

$$R_2 = M \int_0^{+\infty} \log_2 \left(1 + \frac{1}{\Pi_2} \frac{\lambda P_2}{(1+\lambda)\sigma^2} \right) p_{\lambda(\mathfrak{F})}(\lambda; \mu_1, \mu_2, \nu) d\lambda \\ + \bar{M}_2 \int_0^{+\infty} \log_2 \left(1 + \frac{P\lambda}{\Pi_2 \sigma^2} \right) p_{\lambda(\mathfrak{W})}(\lambda; M_2, \bar{M}_2) d\lambda, \quad (34)$$

where μ_1, μ_2 , and ν are given in Table II, and $\Pi = \frac{\Pi_1}{\Pi_2}$.

Proof. Please refer to Appendix A.6. \square

Impact of allowing SIC only at user 2: In the proposed UA-SD MIMO-NOMA, unlike GSVD-based MIMO-NOMA in [22], only user 2 performs SIC, see Section III-C. Hence, when $\lambda < \Pi^{-1}$, the achievable rate of user 1, $R_{1,l}, l = 1, \dots, M$, is limited by the inferior achievable rate at user 2, $R_{1,l}^{(2)}, l = 1, \dots, M$, cf. (74). Based on (74), the potential gain of the achievable ergodic rate of user 1 obtained by allowing SIC at user 1 or 2, as in GSVD-based MIMO-NOMA [22], can be upper bounded as follows:

$$U_1 = \mathbb{E} \left[\sum_{l=1}^M \left(R_{1,l}^{(1)} - R_{1,l} \right) \right] \leq \mathbb{E}_{0 \leq \lambda \leq \Pi^{-1}} \left[\sum_{l=1}^M R_{1,l}^{(1)} \right] \stackrel{(a)}{=} M \int_0^{\Pi^{-1}} \underbrace{\log_2 \left(1 + \frac{1}{\Pi_1} \frac{\frac{P_1}{1+\lambda}}{\sigma^2 + \frac{1}{\Pi_1} \frac{P_2}{1+\lambda}} \right)}_{:=R_U(\lambda)} p_{\lambda(\mathfrak{F})}(\lambda; \mu_1, \mu_2, \nu) d\lambda \\ \stackrel{(b)}{\leq} MK_U \underbrace{\int_0^{\Pi^{-1}} p_{\lambda(\mathfrak{F})}(\lambda; \mu_1, \mu_2, \nu) d\lambda}_{\Pr\{\lambda < \Pi^{-1}\}}, \quad (35)$$

where $K_U = \max_{0 \leq \lambda \leq \Pi^{-1}} \{R_U(\lambda)\} < \infty$ is a bounded constant independent of λ , and (a) and (b) follow from Definition 1 and the Hölder's inequality, respectively. From (35), we observe that the integral tends to zero as $\Pi \rightarrow \infty$. Hence, the potential performance gain also approaches zero as $\Pi \rightarrow \infty$.

Approximations based on asymptotic pdfs: A large finite-dimensional approximation of the marginal eigenvalue pdfs for \mathbf{F} and \mathbf{W} , based on the asymptotic analysis in [22], can be given as follows. Let \mathbf{F} be as defined in Theorem 2. Furthermore, let $\rho_1 = \frac{q}{m_1}$ and $\rho_2 = \frac{q}{m_2}, m_1, m_2 > q$. Then, based on [34, Thm. 2.30], [22], an approximation of the marginal eigenvalue pdf of \mathbf{F} in (25) for large but finite m_1, m_2 , and q is given by

$$\bar{p}_{\lambda(\mathfrak{F})}(\lambda; \rho_1, \rho_2) = \begin{cases} \frac{(1-\rho_1)\sqrt{(\lambda-l_f)(u_f-\lambda)}}{2\pi\rho_1\lambda(\lambda+1)} & \text{if } l_f \leq \lambda \leq u_f \\ 0 & \text{otherwise,} \end{cases} \quad (36)$$

where $l_f = \frac{\rho_1}{\rho_2} \frac{1-\sqrt{1-(1-\rho_1)(1-\rho_2)}}{(1-\rho_1)^2}$ and $u_f = \frac{\rho_1}{\rho_2} \frac{1+\sqrt{1-(1-\rho_1)(1-\rho_2)}}{(1-\rho_1)^2}$ denote the limits of the support. Next, let \mathbf{W} be defined as in Theorem 3. Furthermore, let $\xi = \frac{q}{p}, p > q$. Then, based on [34,

Thm. 2.35], an approximation of the marginal eigenvalue pdf of \mathbf{W} in (29) for large but finite p and q is given by

$$\bar{p}_{\lambda(\mathfrak{W})}(\lambda; \xi) = \begin{cases} \frac{\sqrt{(x-l_w)(u_w-x)}}{2\pi\xi\lambda p} & \text{if } l_w \leq \lambda \leq u_w \\ 0 & \text{otherwise,} \end{cases} \quad (37)$$

where $l_w = p(1 - \sqrt{\xi})^2$ and $u_w = p(1 + \sqrt{\xi})^2$ denote the limits of the support. Approximate ergodic rate expressions \bar{R}_1 and \bar{R}_2 based on (31)-(34) can be obtained by replacing the densities $p_{\lambda(\mathfrak{F})}(\lambda; m_1, m_2, q)$ and $p_{\lambda(\mathfrak{W})}(\lambda; p, q)$ by $\bar{p}_{\lambda(\mathfrak{F})}(\lambda; \rho_1, \rho_2)$ and $\bar{p}_{\lambda(\mathfrak{W})}(\lambda; \xi)$, respectively.

Remark 6. The pdf $\bar{p}_{\lambda(\mathfrak{F})}(\lambda; \rho_1, \rho_2)$ does not exist for the case $\rho_1 = 1$, which is an important case for MIMO-NOMA, as l_f and u_f are infinity⁵.

B. Unequal Power Allocation

In this section, we derive simplified ergodic rate expressions for UPA based on finite-size RMT. In UPA, the powers allocated to the SISO-NOMA symbols $s_l, l = 1, \dots, M$, need not be identical. However, identical powers are allocated to the remaining user symbols⁶, as described in the following. For symbols $s_l, l = 1, \dots, M$, transmit powers $p_{1,l}$ and $p_{2,l}$ are allocated to users 1 and 2, respectively. Furthermore, the \bar{M}_1 symbols $s_l, l = M + 1, \dots, M + \bar{M}_1$, are allocated a transmit power of p_1 . Lastly, the \bar{M}_2 symbols $s_l, l = M + \bar{M}_1 + 1, \dots, L$, are allocated a transmit power of p_2 .

Proposition 6. *For UPA, (3) simplifies as follows:*

$$P_T = \frac{M_1}{NM} \sum_{l=1}^M (p_{1,l} + p_{2,l}) + p_1 \frac{\bar{M}_1}{M} + p_2 \mathbb{1}_{\{\bar{M}_2 > 0\}}, \quad (38)$$

if $M_1 + M_2 > N$, and $P_T = p_1 + p_2$ otherwise.

Proof. Please refer to Appendix A.7. □

Next, we introduce the following definition to simplify the ergodic rate expressions.

⁵This is because, in the asymptotic regime, for $\rho_1 = 1$, \mathbf{F} entails the inversion of an asymptotic square matrix resulting, with probability 1, in eigenvalues which are $+\infty$.

⁶Although we restrict ourselves to non-equal powers only for the SISO-NOMA symbols, the techniques presented in this section can be utilized to extend the analysis to non-equal powers for all symbols in a straightforward manner.

Definition 2 (Based on [30], [35]). Let \mathbf{X} be a $q \times q$ Hermitian symmetric random matrix with eigenvalues $\lambda_1 \geq \lambda_2 \geq \dots \geq \lambda_q$, and let $\boldsymbol{\lambda} = \{\lambda_n, n = 1, \dots, q\}$. Furthermore, let the joint pdf of the eigenvalues be denoted by $p_{\boldsymbol{\lambda}}(\boldsymbol{\lambda})$. Then, the l -th ordered eigenvalue pdf is defined as

$$p_l(\lambda_l) = \int_{\lambda_l}^{+\infty} \dots \int_{\lambda_2}^{+\infty} \left[\int_0^{\lambda_l} \dots \int_0^{\lambda_{q-1}} p_{\boldsymbol{\lambda}}(\boldsymbol{\lambda}) d\lambda_q \dots d\lambda_{l+1} \right] d\lambda_1 \dots d\lambda_{l-1}. \quad (39)$$

Using the above definition, for a $q \times q$ Hermitian symmetric random matrix \mathbf{X} with eigenvalues $\lambda_1, \lambda_2, \dots, \lambda_q$, we may simplify the expectation of a generic additively separable function

$$f(\lambda_1, \dots, \lambda_q) = \sum_{l=1}^q g_l(\lambda_l) \quad (40)$$

in the eigenvalues of \mathbf{X} as

$$\mathbb{E}[f(\lambda_1, \dots, \lambda_q)] = \mathbb{E} \left[\sum_{l=1}^q g_l(\lambda_l) \right] \stackrel{(a)}{=} \sum_{l=1}^q \int_0^{+\infty} g_l(\lambda_l) p_l(\lambda_l) d\lambda_l, \quad (41)$$

where (a) is obtained using Definition 2. In the following, (41) is used to simplify the achievable ergodic rates of the users in terms of the ordered eigenvalue pdfs for UPA.

Based on Proposition 3, the ordered eigenvalue pdf of \mathbf{F} , denoted by $p_l(\lambda_l; \mu_1, \mu_2, \nu)$, which is later utilized to simplify the expressions for $R_{1,l}$ and $R_{2,l}$, $l = 1, \dots, M$, via (41) is given in the following theorem.

Theorem 4. Let $\mathbf{X} \sim \mathcal{CW}_q(m_1, \mathbf{I}_q)$ and $\mathbf{Y} \sim \mathcal{CW}_q(m_2, \mathbf{I}_q)$ be $q \times q$ independent complex-valued Wishart random matrices with $m_1, m_2 \geq q$ degrees of freedom. The pdf of the l -th ordered eigenvalue of matrix $\mathbf{F} = \mathbf{Y}^{\frac{1}{2}} \mathbf{X}^{-1} \mathbf{Y}^{\frac{1}{2}}$ is given by

$$p_l(\lambda_l; m_1, m_2, q) = K_{p_l} g_l^{[l, (), ()]}(\lambda_l; m_1, m_2, q), \quad (42)$$

where K_{p_l} is a constant ensuring that the integral over the pdf is equal to one, and function $g_l^{[d, \mathbf{n}, \mathbf{m}]}(\lambda_l; m_1, m_2, q)$ is given by the recurrence relation

$$\sum_{i=1}^{|\mathcal{I}^{[d, \mathbf{n}]}|} \sum_{j=1}^{|\mathcal{I}^{[d, \mathbf{m}]}|} g_i^{[d-1, \mathbf{n}', \mathbf{m}']}(\lambda_l; m_1, m_2, q), \quad (43)$$

$[l, (), ()]$ denotes the initial value of $[d, \mathbf{n}, \mathbf{m}]$, and “ $()$ ” denotes the empty tuple. Tuples \mathbf{n} and \mathbf{m} are updated as $\mathbf{n}' := \mathbf{n} \cup \{(i, [\mathcal{I}^{[d, \mathbf{n}]}]_i)\}$ and $\mathbf{m}' := \mathbf{m} \cup \{(j, [\mathcal{I}^{[d, \mathbf{m}]}]_j)\}$, where i and j are the summation indices in (43), and $[\mathcal{I}^{[d, \mathbf{n}]}]_i$ and $[\mathcal{I}^{[d, \mathbf{m}]}]_j$ are the i -th and j -th elements of sets $\mathcal{I}^{[d, \mathbf{n}]}$ and $\mathcal{I}^{[d, \mathbf{m}]}$, respectively, defined as $\mathcal{I}^{[d, \mathbf{n}]} := \{1, 2, \dots, q\} \setminus \pi_2(\mathbf{n})$ and $\mathcal{I}^{[d, \mathbf{m}]} := \{1, 2, \dots, q\} \setminus \pi_2(\mathbf{m})$.

Next, the termination step is

$$g_l^{[1, \mathbf{n}, \mathbf{m}]}(\lambda_l; m_1, m_2, q) = \sum_{i=1}^{|\mathcal{I}^{[d, \mathbf{n}]}|} \sum_{j=1}^{|\mathcal{I}^{[d, \mathbf{m}]}|} s(\mathbf{n}', \mathbf{m}') \frac{\lambda_l^{n+m-2+m_2-q}}{(1 + \lambda_l)^{m_1+m_2}} \det \left(\Xi(l, m_1, m_2, q, \mathcal{I}^{[d+1, \mathbf{n}']}, \mathcal{I}^{[d+1, \mathbf{m}']}) \right)$$

TABLE III: Expressions for the pdf in Theorem 4 for various m_1, m_2 , and q .

(m_1, m_2, q)	$p_l(\lambda_l; m_1, m_2, q)$	(m_1, m_2, q)	$p_l(\lambda_l; m_1, m_2, q)$
$(3, 3, 1), l = 1$	$\frac{30\lambda_1}{(1+\lambda_1)^6}$	$(4, 4, 4), l = 1$	$\frac{16\lambda_1^{15}}{(\lambda_1+1)^{17}}$
$(4, 1, 1), l = 1$	$\frac{4}{(1+\lambda_1)^5}$	$(4, 4, 4), l = 2$	$\frac{16\lambda_2^8(100\lambda_2^4+450\lambda_2^3+828\lambda_2^2+700\lambda_2+225)}{(\lambda_2+1)^{17}}$
$(3, 3, 2), l = 1$	$\frac{12\lambda_1^5(5+3\lambda_1)}{(1+\lambda_1)^9}$	$(4, 4, 4), l = 3$	$\frac{16\lambda_3^3(225\lambda_3^4+700\lambda_3^3+828\lambda_3^2+450\lambda_3+100)}{(\lambda_3+1)^{17}}$
$(3, 3, 2), l = 2$	$\frac{12\lambda_2(5+3\lambda_2)}{(1+\lambda_2)^9}$	$(4, 4, 4), l = 4$	$\frac{16}{(\lambda_4+1)^{17}}$

$$\times \prod_{i=1}^{l-1} (-1)^{[\mathcal{I}^{[d, \mathbf{n}]]_i + [\mathcal{I}^{[d, \mathbf{m}]]_i + 1 - m_1 - q}} \text{B}(-\lambda_l^{-1}, 1 + m_1 - [\mathcal{I}^{[d, \mathbf{n}]]_i - [\mathcal{I}^{[d, \mathbf{m}]]_i + q, 1 - m_1 - m_2) \quad (44)$$

where $\text{B}(\cdot, \cdot, \cdot)$ is the incomplete Beta function, $\Xi(l, m_1, m_2, q, \mathcal{I}^{[d+1, \mathbf{n}']}, \mathcal{I}^{[d+1, \mathbf{m}']})$ is a $(q-l) \times (q-l)$ matrix with elements

$$\left[\frac{\lambda_l^{(m_2 - q + [\mathcal{I}^{[d+1, \mathbf{n}']}]_i + [\mathcal{I}^{[d+1, \mathbf{m}']}]_j - 1)} {}_2F_1(m_1 + m_2, m_2 - q + [\mathcal{I}^{[d+1, \mathbf{n}']}]_i + [\mathcal{I}^{[d+1, \mathbf{m}']}]_j - 1, m_2 - q + [\mathcal{I}^{[d+1, \mathbf{n}']}]_i + [\mathcal{I}^{[d+1, \mathbf{m}']}]_j; -\lambda_l) \right]_{ij}, \quad (45)$$

with $i, j = 1, \dots, q-l$,

$$s(\mathbf{n}', \mathbf{m}') = (-1)^{\sum_{i=1}^{|\mathbf{n}'|} [\pi_1(\mathbf{n}')_i] + [\pi_1(\mathbf{m}')_i]}, \quad (46)$$

and ${}_2F_1(\cdot, \cdot; \cdot)$ denotes the Gaussian hypergeometric function [36].

Proof. Please refer Appendix A.8. □

Remark 7. Although the expressions given in Theorem 4 for $p_l(\lambda_l; m_1, m_2, q)$ are cumbersome, the resulting pdfs are simple polynomial expressions. A few examples are given in Table III.

The ordered eigenvalue pdf and the marginal eigenvalue pdf are related as specified in the following corollary.

Corollary 5. *The marginal eigenvalue pdf given in Theorem 2, $p_{\lambda(\mathfrak{F})}(\lambda; m_1, m_2, q)$, and the ordered eigenvalue pdf given in Theorem 4, $p_l(\lambda_l; m_1, m_2, q)$, are related as follows:*

$$p_{\lambda(\mathfrak{F})}(\lambda; m_1, m_2, q) = \frac{1}{q} \sum_{l=1}^q p_l(\lambda; m_1, m_2, q). \quad (47)$$

Proof. The proof follows directly from Definitions 1 and 2. □

Next, we show that based on the ordered eigenvalue pdf for λ_l given in Theorem 4, the expressions in (19) can be simplified.

Proposition 7. For UPA and $M_1 + M_2 \leq N$, the ergodic rates of users 1 and 2 for the proposed UA-SD MIMO-NOMA scheme are given by

$$R_1 = \bar{M}_1 \int_0^{+\infty} \log_2 \left(1 + \frac{p_1 \lambda}{\Pi_1 \sigma^2} \right) p_{\lambda(\mathfrak{W})}(\lambda; M_1, \bar{M}_1) d\lambda, \quad (48)$$

$$R_2 = \bar{M}_2 \int_0^{+\infty} \log_2 \left(1 + \frac{p_2 \lambda}{\Pi_2 \sigma^2} \right) p_{\lambda(\mathfrak{W})}(\lambda; M_2, \bar{M}_2) d\lambda, \quad (49)$$

and for UPA and $M_1 + M_2 > N$, the ergodic rates are given by

$$R_1 = \sum_{l=1}^M \int_0^{\Pi^{-1}} \log_2 \left(1 + \frac{1}{\Pi_2} \frac{\frac{\lambda_l p_{1,l}}{1+\lambda_l}}{\sigma^2 + \frac{1}{\Pi_2} \frac{\lambda_l p_{2,l}}{1+\lambda_l}} \right) p_l(\lambda_l; \mu_1, \mu_2, \nu) d\lambda_l \\ + \sum_{l=1}^M \int_{\Pi^{-1}}^{+\infty} \log_2 \left(1 + \frac{1}{\Pi_1} \frac{\frac{p_{1,l}}{1+\lambda_l}}{\sigma^2 + \frac{1}{\Pi_1} \frac{p_{2,l}}{1+\lambda_l}} \right) p_l(\lambda_l; \mu_1, \mu_2, \nu) d\lambda_l + \bar{M}_1 \log_2 \left(1 + \frac{p_1}{\Pi_1 \sigma^2} \right), \quad (50)$$

$$R_2 = \sum_{l=1}^M \int_0^{+\infty} \log_2 \left(1 + \frac{1}{\Pi_2} \frac{\lambda_l p_{2,l}}{(1+\lambda_l) \sigma^2} \right) p_l(\lambda_l; \mu_1, \mu_2, \nu) d\lambda_l \\ + \bar{M}_2 \int_0^{+\infty} \log_2 \left(1 + \frac{p_2 \lambda}{\Pi_2 \sigma^2} \right) p_{\lambda(\mathfrak{W})}(\lambda; M_2, \bar{M}_2) d\lambda, \quad (51)$$

where μ_1, μ_2 , and ν are given in Table II, and $\Pi = \frac{\Pi_1}{\Pi_2}$.

Proof. Analogous to the proof for Proposition 5, for UPA, (19) can be simplified to (48) and (49) for $M_1 + M_2 \leq N$ based on Proposition 4 and Definition 1. For $M_1 + M_2 > N$, (50) and (51) can be obtained based on (74), Propositions 3 and 4, and Definition 2. \square

Remark 8. From Corollary 5, we note that the proposed UA-SD MIMO-NOMA scheme with EPA could also be analyzed using the ordered eigenvalue pdfs. However, the ergodic rate expressions based on the marginal eigenvalue pdf given in (33) and (34) can be computed more efficiently than the corresponding expressions based on the ordered eigenvalue pdfs given in (50) and (51).

C. Power Allocation Algorithm

In this section, to limit the additional complexity introduced by power allocation, we develop a long-term power allocation algorithm for maximization of the weighted ergodic sum rate, which depends only on the channel statistics.

First, based on (48)-(51), we formulate optimization problem P1 for maximization of the weighted ergodic sum rate as follows:

$$\text{P1: } \max_{p_1, p_2, p_{k,l} \geq 0 \forall k,l} \eta R_1 + (1 - \eta) R_2 \quad \text{s.t.} \quad P_T \leq P_{\max}, \quad (52)$$

where $\eta \in [0, 1]$ is a fixed weight which can be chosen to adjust the rates of user 1 and 2 [37, Sec. 4], and P_{\max} is the available transmit power budget. For $M_1 + M_2 \leq N$, problem P1 is convex. However, for $M_1 + M_2 > N$, problem P1 is non-convex, due to the coupling between $p_{1,l}$ and $p_{2,l}$, $l = 1, \dots, M$, in R_1 given in (50). Hence, efficient convex optimization methods cannot be used for obtaining the global maximum. Instead, for $M_1 + M_2 > N$, we utilize the low-complexity concave-convex procedure (CCP) [38], [39] to obtain a suboptimal solution.

To this end, we replace R_1 by a concave overestimator, denoted by \tilde{R}_1 , obtained via a first-order approximation of the non-concave terms around $p_{2,l} = q_l$, $l = 1 \dots, M$, given (excluding constant terms) by

$$\tilde{R}_1 = \sum_{l=1}^M \int_0^{\Pi^{-1}} \log_2 \left(1 + \frac{\lambda_l p_{1,l}}{\Pi_2 \sigma^2 (1 + \lambda_l)} + \frac{\lambda_l p_{2,l}}{\Pi_2 \sigma^2 (1 + \lambda_l)} \right) p_l(\lambda_l; \mu_1, \mu_2, \nu) d\lambda_l \\ + \sum_{l=1}^M \int_{\Pi^{-1}}^{+\infty} \log_2 \left(1 + \frac{p_{1,l}}{\Pi_1 \sigma^2 (1 + \lambda_l)} + \frac{p_{2,l}}{\Pi_1 \sigma^2 (1 + \lambda_l)} \right) p_l(\lambda_l; \mu_1, \mu_2, \nu) d\lambda_l + L_1 + \bar{M}_1 \log_2 \left(1 + \frac{p_1}{\Pi_1 \sigma^2} \right), \quad (53)$$

$$L_1 = -\frac{1}{\log(2)} \sum_{l=1}^M \left[\int_0^{\Pi^{-1}} \frac{\lambda_l (p_{2,l} - q_l)}{\lambda_l q_l + \Pi_2 \sigma^2 (1 + \lambda_l)} p_l(\lambda_l; \mu_1, \mu_2, \nu) d\lambda_l + \int_{\Pi^{-1}}^{+\infty} \frac{(p_{2,l} - q_l)}{q_l + \Pi_1 \sigma^2 (1 + \lambda_l)} p_l(\lambda_l; \mu_1, \mu_2, \nu) d\lambda_l \right]. \quad (54)$$

Next, we construct a concave optimization problem P2, based on \tilde{R}_1 , as follows:

$$\text{P2:} \quad \max_{p_1, p_2, p_{k,l} \geq 0 \forall k,l} \eta \tilde{R}_1 + (1 - \eta) R_2 \quad \text{s.t.} \quad P_T \leq P_{\max}, \quad (55)$$

which is solved iteratively. First, we initialize $q_l^{(0)} = 0$, $l = 1, \dots, M$. Next, in iteration $n = 1, 2, \dots$, we solve P2 given $q_l^{(n-1)}$ to obtain the optimal solution $p_1^{(n)}, p_2^{(n)}, p_{k,l}^{(n)}$, $k = 1, 2, l = 1, \dots, M$. Then, we update $q_l^{(n)} = p_{2,l}^{(n)}$, $l = 1, \dots, M$, to obtain a tighter concave overestimator in the next iteration. The iterations are continued until convergence, upto a suitable numerical tolerance ϵ . The CCP is guaranteed to converge to a stationary point of P1 [38], [39]. The proposed algorithm is summarized in Algorithm 1.

V. SIMULATION RESULTS

In this section, we first verify the pdf expressions in Theorems 2 and 4. Then, we compare the ergodic achievable rate regions of the proposed UA-SD MIMO-NOMA for EPA and UPA with those of GSVD-based MIMO-NOMA [22] and OMA.

A. Probability Density Functions

Figure 1 compares the marginal eigenvalue pdf, $p_{\lambda(\mathfrak{F})}(\lambda; m_1, m_2, q)$, derived in Theorem 2 for $m_1 = 5, m_2 = 4$, and $q = 2$, with the empirical pdf obtained via Monte Carlo simulation and

Algorithm 1 Power Allocation Algorithm for UPA and $M_1 + M_2 > N$.

- 1: Initialize $q_l^{(0)} = 0$, $p_1^{(0)} = p_2^{(0)} = p_{k,l}^{(0)} = -\infty$ for $k = 1, 2, l = 1, \dots, M$, numerical tolerance ϵ , and iteration index $n = 0$
 - 2: **repeat**
 - 3: $n \leftarrow n + 1$
 - 4: Solve P2 given $q_l^{(n-1)}$, $l = 1, \dots, M$, to obtain the solution $p_1^{(n)}, p_2^{(n)}, p_{k,l}^{(n)} \forall k, l$
 - 5: Update $q_l^{(n)} = p_{2,l}^{(n)}$, $l = 1, \dots, M$, for the next iteration
 - 6: **until** $|p_1^{(n)} - p_1^{(n-1)}| < \epsilon$, $|p_2^{(n)} - p_2^{(n-1)}| < \epsilon$, and $|p_{k,l}^{(n)} - p_{k,l}^{(n-1)}| < \epsilon \forall k, l$
 - 7: Return $p_1^{(n)}, p_2^{(n)}, p_{k,l}^{(n)}$, $k = 1, 2, l = 1, \dots, M$, as the power allocation
-

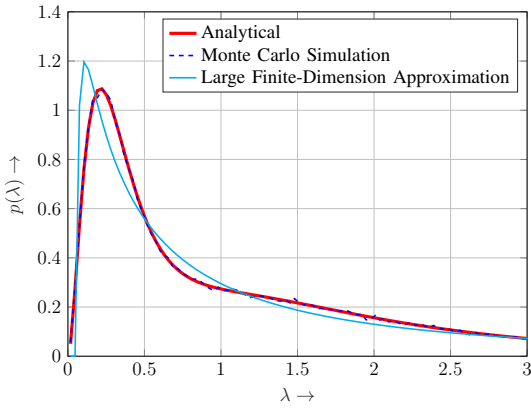


Fig. 1: Simulation of the pdf given in Theorem 2 for $m_1 = 5, m_2 = 4$, and $q = 2$.

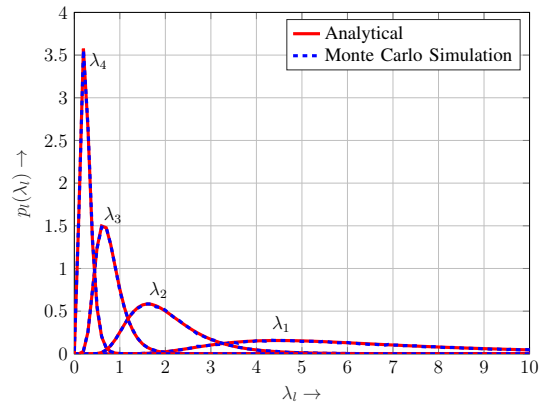


Fig. 2: Simulation of the pdf given in Theorem 4 for $m_1 = 7, m_2 = 8$, and $q = 4$.

the approximation based on the asymptotic pdf given in (36). From the figure, we note that the derived analytical result is in perfect agreement with the numerical simulation. However, for the considered small finite values of m_1, m_2 , and q , the approximation based on the asymptotic pdf does not result in an accurate fit.

Analogously, Figure 2 compares the ordered eigenvalue pdfs, $p_l(\lambda_l; m_1, m_2, n)$, $l = 1, \dots, 4$, derived in Theorem 4 for $m_1 = 7, m_2 = 8$, and $q = 4$, with empirical pdfs obtained via Monte Carlo simulation. We observe also in this case that the derived analytical results are in excellent agreement with the numerical simulation, thereby validating our derived expressions.

B. Ergodic Rate Regions

For comparing the ergodic rate regions, we assume that the first and second users are located at distances of $d_1 = 100$ m and $d_2 = 10$ m from the BS, respectively. The path loss is modeled as $\Pi_k = d_k^2$, i.e., $\Pi_1 = 100^2$ and $\Pi_2 = 10^2$. Furthermore, we assume a noise variance of $\sigma^2 = -35$ dBm and set $P_T = P_{\max}$ for EPA.

Figure 3 shows the convex hull of the ergodic rate regions of the proposed UA-SD MIMO-NOMA for EPA and UPA, GSVD-based MIMO-NOMA [22], and OMA for the case $\bar{M}_2 > 0$ with $M_1 = M_2 = 3$, $N = 5$, and $P_{\max} = 20$ dBm. For EPA, the rate region is obtained by varying P_1 and P_2 in (33) and (34). For UPA, the rate region is obtained by solving P1 using Algorithm 1 for different $\eta \in [0, 1]$. For GSVD-based MIMO-NOMA, the rates region is obtained based on the asymptotic RMT expressions from [22] which are modified based on our finite-size RMT framework.

First, we note that, in Figure 3 (and in all subsequent figures), the ergodic rate regions obtained analytically via our finite-size RMT results and empirically via Monte Carlo simulation are in perfect agreement, thereby confirming the validity of our theoretical results.

Furthermore, from Figure 3, we observe that the proposed UA-SD MIMO-NOMA outperforms GSVD-based MIMO-NOMA for both EPA and UPA as channel inversion at the BS for $\bar{M}_2 = 2$ symbols, $s_{2,l}$, $l = 4, 5$, of user 2 is avoided. UA-SD MIMO-NOMA also outperforms OMA for a wide range of user rates. However, OMA is superior for the rate pairs close to the single-user (SU)-MIMO rates due to the sustained channel inversion in the proposed scheme for the first $M + \bar{M}_1$ symbols, s_1 and $s_{1,l}$, $l = 2, 3$. Nevertheless, a hybrid scheme performing time sharing between the proposed UA-SD MIMO-NOMA and SU-MIMO, as exemplarily shown for UPA, outperforms OMA over the entire rate region. Moreover, as expected, for the proposed UA-SD MIMO-NOMA, optimal UPA outperforms EPA. Lastly, the ergodic rate region obtained based on the asymptotic pdfs in (36) and (37) accurately approximates the ergodic rate region of the proposed UA-SD MIMO-NOMA with EPA.

Figure 4 shows the convex hull of the ergodic rate regions of the same schemes as considered in Figure 3 for the case $M_1 + M_2 = N$ with $M_1 = M_2 = 2$, $N = 4$, and $P_{\max} = 20$ dBm. As no symbols s_l are transmitted to both users, for EPA, no rate adjustment between the users is possible. Furthermore, as $M_1 + M_2 = N$, the achievable rate for GSVD-based MIMO-NOMA is zero as explained in Section II-B. On the other hand, the proposed UA-SD MIMO-NOMA

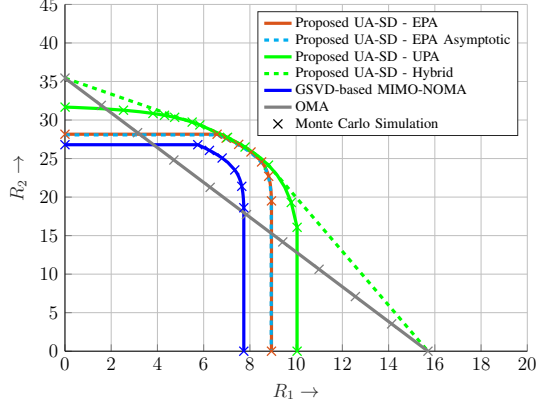


Fig. 3: Ergodic rate region for $M_1 = 3, M_2 = 3, N = 5$, and $P_{\max} = 20$ dBm.

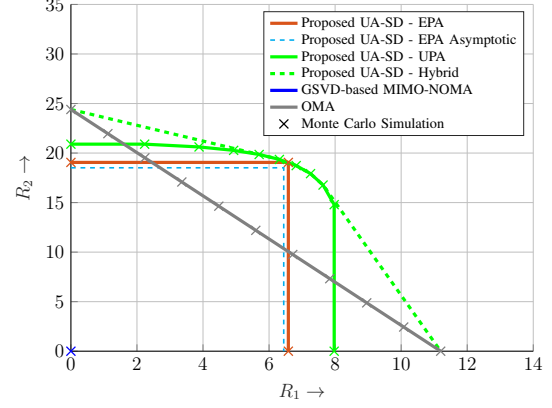


Fig. 4: Ergodic rate region for $M_1 = 2, M_2 = 2, N = 4$, and $P_{\max} = 20$ dBm.

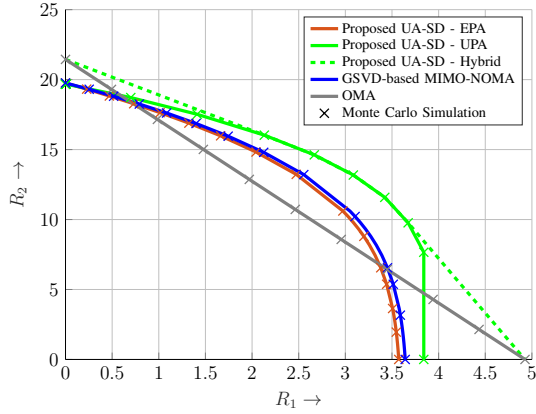


Fig. 5: Ergodic rate region for $M_1 = 3, M_2 = 3, N = 3$, and $P_{\max} = 10$ dBm.

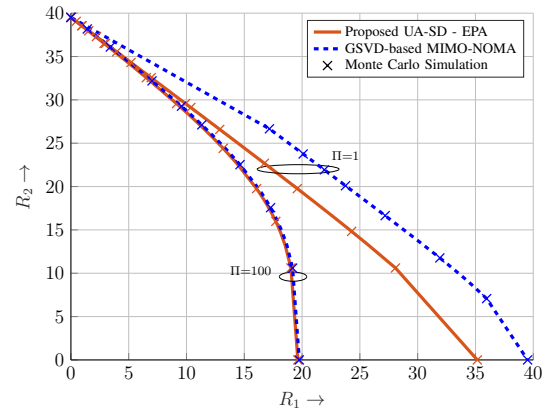


Fig. 6: Ergodic rate region for $M_1 = 3, M_2 = 3, N = 3$, $P_{\max} = 30$ dBm, and $\Pi = 1$ and 100.

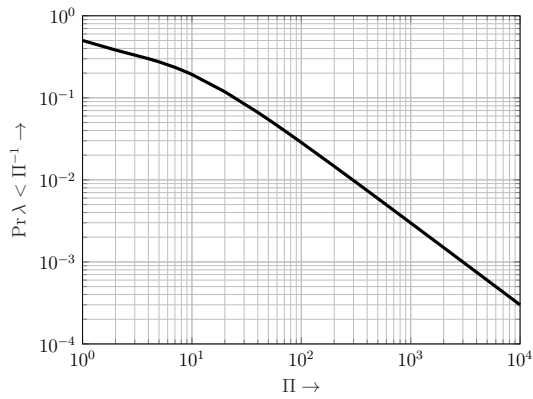


Fig. 7: Plot of $\Pr \{ \lambda < \Pi^{-1} \}$ for $M_1 = 3, M_2 = 3$, and $N = 3$ as a function of Π .

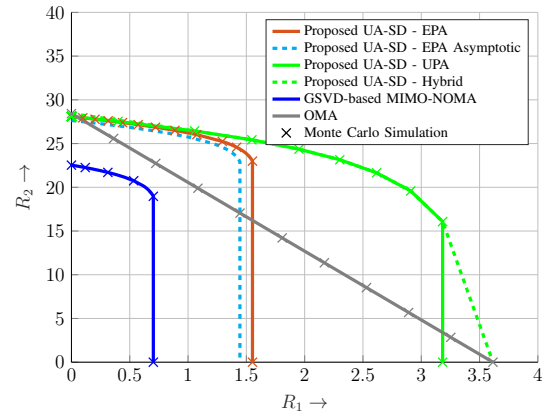


Fig. 8: Ergodic rate region for $M_1 = 1, M_2 = 4, N = 4$, and $P_{\max} = 10$ dBm.

significantly outperforms OMA for a wide range of user rates as it exploits BD, and the proposed hybrid scheme outperforms OMA over the entire rate region. Moreover, unlike EPA, UPA allows the adjustment of the user rates. Lastly, for EPA, the ergodic rate region obtained based on the asymptotic pdfs approximates the ergodic rate region of the proposed UA-SD MIMO-NOMA upto a small gap.

Figure 5 shows the ergodic rate region for the case $\bar{M}_2 = 0$ with $M_1 = M_2 = N = 3$, and $P_{\max} = 10$ dBm, where all spatial streams are shared by the two users via SISO-NOMA. In this case, the proposed UA-SD MIMO-NOMA with UPA outperforms GSVD-based MIMO-NOMA. Furthermore, the proposed scheme with UPA outperforms OMA for a wide range of user rates, and the proposed hybrid scheme outperforms OMA over the entire rate region. Lastly, for the considered case, GSVD-based MIMO-NOMA yields a marginally larger rate region than UA-SD MIMO-NOMA with EPA, which restricts SIC to user 2 limiting the achievable ergodic rate of user 1, $R_{1,l}, l = 1, \dots, M$, to the inferior rate at user 2, $R_{1,l}^{(2)}, l = 1, \dots, M$, cf. Section IV-A. In the following, this effect is investigated in detail.

Figure 6 compares the rate regions of the proposed UA-SD MIMO-NOMA with EPA, which restricts SIC to user 2, and GSVD-based MIMO-NOMA, which allows SIC at users 1 and 2, cf. Section III-C, for $P_{\max} = 30$ dBm, and $\Pi = 1$ and 100. From the figure, we observe that the significant performance loss for $\Pi = 1$ reduces to a negligible performance loss for $\Pi = 100$, thereby suggesting that for large Π , the potential performance benefit from allowing SIC at users 1 and 2, as in GSVD-based MIMO-NOMA, is insignificant. Furthermore, as Π increases, the potential performance gain decreases rapidly as it is proportional to $\Pr\{\lambda < \Pi^{-1}\}$, cf. Section IV-A, which also falls rapidly as Π increases, as shown in Figure 7.

Figure 8 shows the convex hull of the ergodic rate region for the case $M_1 \neq M_2, \bar{M}_2 > 0$, with $M_1 = 1, M_2 = N = 4$, and $P_{\max} = 10$ dBm. In this case, we observe that the proposed UA-SD MIMO-NOMA with EPA and UPA outperform GSVD-based MIMO-NOMA as they avoid channel inversion, cf. Section II-B3. Furthermore, the proposed UA-SD MIMO-NOMA with UPA significantly outperforms EPA. Moreover, for EPA, the rate region obtained based on the asymptotic pdf has a small gap to the exact result as $M_1 = 1$ is small.

VI. CONCLUSION

We proposed a UA-SD MIMO-NOMA scheme based on a new matrix decomposition that achieves SD through a combination of precoder design and low-complexity self-interference

cancellation at the users, thereby lowering the decoding complexity at the users compared to joint decoding. Furthermore, we derived ergodic rate expressions for the proposed scheme for EPA and UPA based on a finite-size RMT framework. We exploited the derived ergodic rate expressions to develop a long-term power allocation algorithm for the proposed scheme which only depends on the channel statistics. Our performance comparisons based on the ergodic achievable rate regions revealed that the proposed scheme with EPA and UPA outperforms GSVD-based MIMO-NOMA [22] and OMA for most user rate combinations by avoiding channel inversion at the transmitter. Furthermore, a hybrid scheme employing time sharing enhanced the performance even further. Lastly, as in SISO-NOMA [3], the benefits of the proposed scheme are fully exploited when the ratio of the path loss coefficients of the users is large.

APPENDIX A: PROOFS

A.1: Proof of Proposition 1

For $M_1 + M_2 > N$, from (7), noting that, in this case, \mathbf{Z} is invertible, we have

$$\mathbf{H}_1^H \mathbf{H}_1 + \mathbf{H}_2^H \mathbf{H}_2 = (\mathbf{Z}^{-1})^H (\mathbf{C}^H \mathbf{C} + \mathbf{S}^H \mathbf{S}) \mathbf{Z}^{-1} = (\mathbf{Z}^{-1})^H \mathbf{Z}^{-1} = (\mathbf{Z} \mathbf{Z}^H)^{-1}. \quad (56)$$

Hence, (3) can be simplified to

$$P_T \stackrel{(a)}{=} P_{\text{tr}}(\mathbb{E}[\mathbf{Z} \mathbf{Z}^H]) = P_{\text{tr}}\left(\mathbb{E}\left[\underbrace{(\mathbf{H}_1^H \mathbf{H}_1 + \mathbf{H}_2^H \mathbf{H}_2)^{-1}}_{\mathbf{W}}\right]\right) = P_{\text{tr}}(\mathbb{E}[\hat{\mathbf{W}}]), \quad (57)$$

where (a) is obtained by setting $\mathbf{P} = \mathbf{Z}$ in (3), noting that $p_{1,l} + p_{2,l} = P, l = 1, \dots, L$, and exploiting $\mathbb{E}[\text{tr}(\mathbf{Z}^H \mathbf{Z})] = \text{tr}(\mathbb{E}[\mathbf{Z} \mathbf{Z}^H])$. Matrix $\hat{\mathbf{W}} \sim \mathcal{CW}_N(M_1 + M_2, \mathbf{I}_N)$ [40, Thm. 3.3.8]. By applying [40, Lemma 3.2 (ii)], we obtain

$$P_T = \frac{PL}{N - (M_1 + M_2)}. \quad (58)$$

Proceeding analogously for $M_1 + M_2 \leq N$ and combining the results, we obtain the expression in (9). \square

A.2: Proof of Theorem 1

For $M_1 + M_2 \leq N$, matrices $\mathbf{Q}_1, \mathbf{Q}_2$, and \mathbf{Z} are obtained using BD as described in Section II-B2, [25, Sec. III].

For $M_1 + M_2 > N$, we have $L = N$. Let $\mathbf{K} \in \mathbb{C}^{N \times M}$ denote a matrix containing the basis vectors of the M dimensional space $\text{null}\left(\left[\bar{\mathbf{H}}_1 \quad \bar{\mathbf{H}}_2\right]^H\right) \cap \text{col}(\mathbf{H}_1^H) \cap \text{col}(\mathbf{H}_2^H)$, which exists

when $M > 0$. For the first user, matrix $\tilde{\mathbf{H}}_1 = \mathbf{H}_1 \begin{bmatrix} \mathbf{K} & \bar{\mathbf{H}}_2 \end{bmatrix}$ is forced to the identity matrix by using SVD. Let

$$\tilde{\mathbf{H}}_1 = \hat{\mathbf{U}}_1 \mathbf{\Sigma}_1 \hat{\mathbf{V}}_1^H, \quad (59)$$

where $\hat{\mathbf{U}}_1 \in \mathbb{C}^{M_1 \times M_1}$ and $\hat{\mathbf{V}}_1 \in \mathbb{C}^{M_1 \times M_1}$ are unitary matrices, and $\mathbf{\Sigma}_1 \in \mathbb{R}^{M_1 \times M_1}$ is a diagonal matrix which has the singular values of $\tilde{\mathbf{H}}_1$ on its main diagonal. Note that $\hat{\mathbf{U}}_1^H \tilde{\mathbf{H}}_1 (\hat{\mathbf{V}}_1 \mathbf{\Sigma}_1^+)^T = \mathbf{I}_{M_1}$.

Next, for the second user, matrix $\hat{\mathbf{H}}_2 = \mathbf{H}_2 \bar{\mathbf{H}}_1$ is diagonalized using SVD. Let

$$\hat{\mathbf{H}}_2 = \hat{\mathbf{U}}_2 \mathbf{\Sigma}_2 \hat{\mathbf{V}}_2^H, \quad (60)$$

where $\hat{\mathbf{U}}_2 \in \mathbb{C}^{M_2 \times M_2}$ and $\hat{\mathbf{V}}_2 \in \mathbb{C}^{\bar{M}_2 \times \bar{M}_2}$ are unitary matrices, and $\mathbf{\Sigma}_2 \in \mathbb{R}^{M_2 \times \bar{M}_2}$ is a diagonal matrix which has the singular values of $\hat{\mathbf{H}}_2$ on its main diagonal. As a result, $\hat{\mathbf{U}}_2^H \hat{\mathbf{H}}_2 \hat{\mathbf{V}}_2 = \mathbf{\Sigma}_2$ is a diagonal matrix.

Furthermore, for the second user, matrix

$$\tilde{\mathbf{H}}_2 = \hat{\mathbf{U}}_2^H \left(\mathbf{H}_2 \begin{bmatrix} \mathbf{K} & \bar{\mathbf{H}}_2 \end{bmatrix} \right) (\hat{\mathbf{V}}_1 \mathbf{\Sigma}_1^+)^T \quad (61)$$

is diagonalized in two steps. First, QR decomposition is used to zero-out the last \bar{M}_1 columns of $\tilde{\mathbf{H}}_2$. Next, SVD is used to diagonalize the remaining columns.

Let, by QR decomposition, $\tilde{\mathbf{H}}_2^H = \mathbf{Q}\mathbf{R}$, where $\mathbf{Q} \in \mathbb{C}^{M_1 \times M_1}$ is a unitary matrix, and $\mathbf{R} \in \mathbb{C}^{M_1 \times M_2}$ is a rank M upper triangular matrix. If M is zero, then $\mathbf{Q} = \mathbf{I}_{M_1}$ and $\mathbf{R} = \mathbf{0}$. In either case, $\tilde{\mathbf{H}}_2 \mathbf{Q}$ is a matrix with the last \bar{M}_1 columns equal to zero.

Lastly, the $(M_1 + M_2 - N) \times M$ matrix obtained by taking the last $M_1 + M_2 - N$ rows and the first M columns of $\tilde{\mathbf{H}}_2 \mathbf{Q}$, denoted by \mathbf{B}_3 , is diagonalized applying again SVD. Let

$$\mathbf{B}_3 = \hat{\mathbf{U}}_3 \mathbf{\Sigma} \hat{\mathbf{V}}_3^H, \quad (62)$$

where $\hat{\mathbf{U}}_3 \in \mathbb{C}^{M \times M}$ and $\hat{\mathbf{V}}_3 \in \mathbb{C}^{M \times M}$ are unitary matrices, and $\mathbf{\Sigma} \in \mathbb{R}^{M \times M}$ is a diagonal matrix which has the singular values of \mathbf{B}_3 on its main diagonal. The diagonal entries of $\mathbf{\Sigma}$ are the M GSVs of \mathbf{H}_2 and \mathbf{H}_1 as shown in Appendix A.4.

Using the intermediate results from above, we obtain

$$\mathbf{Z} = \begin{bmatrix} \begin{bmatrix} \mathbf{K} & \bar{\mathbf{H}}_2 \end{bmatrix} \hat{\mathbf{V}}_1 \mathbf{\Sigma}_1^+ \mathbf{Q} \begin{bmatrix} \hat{\mathbf{V}}_3 & \mathbf{0} \\ \mathbf{0} & \mathbf{I}_{\bar{M}_1} \end{bmatrix} \begin{bmatrix} (\mathbf{I}_M + \mathbf{\Sigma})^{-\frac{1}{2}} & \mathbf{0} \\ \mathbf{0} & \mathbf{I}_{\bar{M}_1} \end{bmatrix} & \frac{1}{\sqrt{M_2}} \mathbf{H}_1 \hat{\mathbf{V}}_2 \end{bmatrix}, \quad (63)$$

$$\mathbf{Q}_1 = \begin{bmatrix} \hat{\mathbf{V}}_3^H & \mathbf{0} \\ \mathbf{0} & \mathbf{I}_{\bar{M}_1} \end{bmatrix} \mathbf{Q}^H \hat{\mathbf{U}}_1^H, \quad \mathbf{Q}_2 = \begin{bmatrix} \mathbf{I}_{\bar{M}_2} & \mathbf{0} \\ \mathbf{0} & \hat{\mathbf{U}}_3^H \end{bmatrix} \hat{\mathbf{U}}_2^H. \quad (64)$$

Substituting the above matrices into $\mathbf{Q}_1 \mathbf{H}_1 \mathbf{Z}$ and $\mathbf{Q}_2 \mathbf{H}_2 \mathbf{Z}$, we obtain

$$\mathbf{Q}_1 \mathbf{H}_1 \mathbf{Z} = \begin{bmatrix} \underbrace{(\mathbf{I}_M + \boldsymbol{\Sigma})^{-\frac{1}{2}}}_{:=\boldsymbol{\Sigma}_1} & \mathbf{0} & \mathbf{0} \\ \mathbf{0} & \underbrace{\mathbf{I}_{\bar{M}_1}}_{:=\mathbf{D}_1} & \mathbf{0} \end{bmatrix}, \quad \mathbf{Q}_2 \mathbf{H}_2 \mathbf{Z} = \begin{bmatrix} \underbrace{\mathbf{A}_3 \hat{\mathbf{V}}_3^H (\mathbf{I}_M + \boldsymbol{\Sigma})^{-\frac{1}{2}}}_{:=\mathbf{T}} & \mathbf{0} & \underbrace{\frac{1}{\sqrt{\bar{M}_2}} \hat{\boldsymbol{\Sigma}}_2}_{:=\mathbf{D}_2} \\ \underbrace{\boldsymbol{\Sigma} (\mathbf{I}_M + \boldsymbol{\Sigma})^{-\frac{1}{2}}}_{:=\boldsymbol{\Sigma}_2} & \mathbf{0} & \mathbf{0} \end{bmatrix}, \quad (65)$$

where $\mathbf{A}_3 \in \mathbb{C}^{\bar{M}_2 \times M}$ contains the first \bar{M}_2 rows and the first M columns of $\tilde{\mathbf{H}}_2 \mathbf{Q}$, and $\hat{\boldsymbol{\Sigma}}_2 \in \mathbb{R}^{\bar{M}_2 \times \bar{M}_2}$ contains the first \bar{M}_2 rows of $\boldsymbol{\Sigma}_2$, which leads to (10). \square

A.3: Proof for Proposition 2

For EPA, as the same power is allocated to all symbols, for $M_1 + M_2 \leq N$, based on (6), we have $P_T = 2P$. Next, for $M_1 + M_2 > N$, since $\mathbf{P} = \mathbf{Z}$, (3) simplifies to $P_T = PE [\text{tr}(\mathbf{Z}^H \mathbf{Z})]$. Further, from (63), we have

$$\mathbf{Z} = \begin{bmatrix} \underbrace{\mathbf{K} \mathbf{A}_1 \hat{\mathbf{V}}_3 (\mathbf{I}_M + \boldsymbol{\Sigma})^{-1}}_{:=\mathbf{Z}_1} & \underbrace{\bar{\mathbf{H}}_2 \mathbf{A}_2 \mathbf{I}_{\bar{M}_1}}_{:=\mathbf{Z}_2} & \underbrace{\frac{1}{\sqrt{\bar{M}_2}} \bar{\mathbf{H}}_1 \hat{\mathbf{V}}_2}_{:=\mathbf{Z}_3} \end{bmatrix}, \quad (66)$$

where \mathbf{A}_1 and \mathbf{A}_2 contain M and \bar{M}_1 rows of $\hat{\mathbf{V}}_1 \boldsymbol{\Sigma}_1^+ \mathbf{Q}$, respectively. Hence,

$$\mathbb{E} [\text{tr}(\mathbf{Z}^H \mathbf{Z})] = \mathbb{E} [\text{tr}(\mathbf{Z}_1^H \mathbf{Z}_1)] + \mathbb{E} [\text{tr}(\mathbf{Z}_2^H \mathbf{Z}_2)] + \mathbb{E} [\text{tr}(\mathbf{Z}_3^H \mathbf{Z}_3)]. \quad (67)$$

The individual traces can be found by noting that \mathbf{K} is fully correlated with $\hat{\mathbf{V}}_1$, $\bar{\mathbf{H}}_2$ is uncorrelated from $\hat{\mathbf{V}}_1$, and $\bar{\mathbf{H}}_1 \hat{\mathbf{V}}_2$ is unitary, and simplified based on [40, Thm. 3.3.8] leading to

$$\mathbb{E} [\text{tr}(\mathbf{Z}_1^H \mathbf{Z}_1)] = \frac{M_1}{N}, \quad \mathbb{E} [\text{tr}(\mathbf{Z}_2^H \mathbf{Z}_2)] = \frac{\bar{M}_1}{M}, \quad \mathbb{E} [\text{tr}(\mathbf{Z}_3^H \mathbf{Z}_3)] = 1. \quad (68)$$

Upon substitution of the traces into $P_T = PE [\text{tr}(\mathbf{Z}^H \mathbf{Z})]$, (20) follows. \square

A.4: Proof of Proposition 3

In the following, we consider the case $M_1, M_2 \geq N$. The proofs for the remaining cases specified in Table II follow analogously.

From Appendix A.2, we note that $\boldsymbol{\Sigma}$ contains the singular values of matrix \mathbf{B}_3 in (62). For $M_1, M_2 \geq N$, we have $\bar{\mathbf{H}}_1 = \bar{\mathbf{H}}_2 = \{\}$. As the non-zero singular values of a matrix are unaffected by multiplication with unitary matrices and the conjugate transpose operation, the non-zero singular values of \mathbf{B}_3 , denoted by $\sigma(\mathbf{B}_3)$, can be simplified to

$$\sigma(\mathbf{B}_3) = \sigma(\mathbf{Q}\mathbf{R}) = \sigma(\tilde{\mathbf{H}}_2) \stackrel{(a)}{=} \sigma(\mathbf{H}_2 \mathbf{K} \hat{\mathbf{V}}_1 \boldsymbol{\Sigma}_1^+) \stackrel{(b)}{=} \sigma(\mathbf{H}_2 \mathbf{H}_1^+), \quad (69)$$

where (a) is obtained from (61) and (b) follows by noting that $\hat{\mathbf{V}}_1 \Sigma_1^+ \hat{\mathbf{U}}_1^H = \mathbf{H}_1^+$ and $\mathbf{K} = \mathbf{I}_N$. Hence, the non-zero singular values of \mathbf{B}_3 are the same as those of matrix $\mathbf{H}_2 \mathbf{H}_1^+$, which are the GSVs of \mathbf{H}_2 and \mathbf{H}_1 as they are solutions μ to

$$\det(\mu^2 \mathbf{I}_N - \mathbf{H}_2 (\mathbf{H}_1^H \mathbf{H}_1)^{-1} \mathbf{H}_2) = 0, \quad (70)$$

thereby proving the assertion in Appendix A.2. Furthermore, the squares of the singular values of \mathbf{B}_3 have the same distribution as the eigenvalues of the F-distributed matrix [31], [32] $\mathbf{F} = (\mathbf{W}_2)^{\frac{1}{2}} \mathbf{W}_1^{-1} (\mathbf{W}_2)^{\frac{1}{2}}$, where $\mathbf{W}_2 \sim \mathcal{CW}_N(M_2, \mathbf{I}_M)$ and $\mathbf{W}_1 \sim \mathcal{CW}_N(M_1, \mathbf{I}_M)$ are independent Wishart distributed matrices [23, Thm. 3.2.4, Thm. 3.3.10, and Thm. 3.4.2], [27, Sec. 2], which completes the proof for the case $M_1, M_2 \geq N$.

Lastly, as seen from (65), matrices Σ_1^2 and Σ_2^2 are constructed as $\Sigma_1^2 = (\mathbf{I}_M + \Sigma)^{-1}$ and $\Sigma_2^2 = \Sigma(\mathbf{I}_M + \Sigma)^{-1}$, which yields (24). \square

A.5: Proof of Theorem 2

The density of the matrix-variate F-distribution is given by [23], [31]

$$K_F \frac{\det(\mathbf{F})^{m_2-q}}{\det(\mathbf{I}_q + \mathbf{F})^{m_1+m_2}}, \quad (71)$$

where K_F is a proportionality constant that ensures that the pdf integrates to one. By performing a change of variables to the eigenvalues and eigenvectors of \mathbf{F} , and integrating over the eigenvectors [41, Proposition 1.3.4], we obtain the joint distribution of the real-valued eigenvalues, analogous to the results in [31], [32, Introduction], as follows:

$$K_\lambda \prod_{l=1}^q \frac{\lambda_l^{m_2-q}}{(1 + \lambda_l)^{m_1+m_2}} \prod_{1 \leq j < k \leq q} (\lambda_j - \lambda_k)^2, \quad (72)$$

where $\lambda_1 \geq \lambda_2 \geq \dots \geq \lambda_q$ denote the eigenvalues, and K_λ is a constant ensuring that the integral over the joint eigenvalue pdf is equal to one. Next, in order to obtain the marginal eigenvalue pdf, using Definition 1, we integrate out the $q - 1$ largest eigenvalues. The $q - 1$ dimensional integration is performed using $\phi_i(\lambda_j) = \lambda_j^{i-1}$, $\psi_i(\lambda_j) = \lambda_j^{i-1}$, and $\xi(\lambda) = \frac{\lambda^{m_2-q}}{(1 + \lambda)^{m_1+m_2}}$ in [30, Corollary 1, Theorem 1] to obtain the expression in (25). \square

A.6: Proof of Proposition 5

For $M_1 + M_2 \leq N$, based on Proposition 4, (19) can be simplified to

$$\mathbf{R}_1 = \mathbb{E} \left[\sum_{l=1}^{\bar{M}_1} \mathbf{R}_{1,l}^{(1)} \right], \quad \mathbf{R}_2 = \mathbb{E} \left[\sum_{l=M_1+1}^L \mathbf{R}_{2,l} \right], \quad (73)$$

which are of the form given in (23) and can be simplified to (31) and (32) based on Definition 1.

For $M_1 + M_2 > N$, based on Proposition 3, the condition in (17) can be written in terms of the squares of the GSVs $\lambda_l, l = 1, \dots, M$, as

$$R_{1,l} = \begin{cases} R_{1,l}^{(1)} & \text{if } \lambda_l > \Pi^{-1} \\ R_{1,l}^{(2)} & \text{otherwise.} \end{cases} \quad (74)$$

Hence, based on (74), (19) simplifies to

$$R_1 = E_{\lambda_l > \Pi^{-1}} \left[\sum_{l=1}^M R_{1,l}^{(1)} \right] + E_{\lambda_l < \Pi^{-1}} \left[\sum_{l=1}^M R_{1,l}^{(2)} \right] + E \underbrace{\left[\sum_{l=M+1}^{M+\bar{M}_1} R_{1,l}^{(1)} \right]}_{\text{Deterministic quantity}}, \quad (75)$$

$$R_2 = E \left[\sum_{l=1}^M R_{2,l} \right] + E \left[\sum_{l=M+\bar{M}_1+1}^L R_{2,l} \right], \quad (76)$$

which are, for EPA, of the form given in (23) and can be further simplified to (33) and (34) based on Propositions 3 and 4 and Definition 1. \square

A.7: Proof of Proposition 6

For UPA, (3) can be simplified as follows:

$$P_T = E \left[\text{tr} (\mathbf{P}^H \mathbf{P} \mathbf{D}_P) \right], \quad (77)$$

where $\mathbf{D}_P = \text{diag} \left(p_{1,1} + p_{2,1}, \dots, p_{1,M} + p_{2,M}, \underbrace{p_1, \dots, p_1}_{\bar{M}_1 \text{ times}}, \underbrace{p_2, \dots, p_2}_{\bar{M}_2 \text{ times}} \right)$. For $M_1 + M_2 > N$, based on (66) and (68), the right hand side of (77) simplifies as follows:

$$\sum_{l=1}^M (p_{1,l} + p_{2,l}) \frac{E \left[\text{tr} (\mathbf{Z}_1^H \mathbf{Z}_1) \right]}{M} + p_1 E \left[\text{tr} (\mathbf{Z}_2^H \mathbf{Z}_2) \right] + p_2 E \left[\text{tr} (\mathbf{Z}_3^H \mathbf{Z}_3) \right], \quad (78)$$

which leads to (38). For $M_1 + M_2 \leq N$, based on (6), (77) simplifies to $P_T = p_1 + p_2$. \square

A.8: Proof of Theorem 4

The joint eigenvalue pdf of an F-distributed matrix \mathbf{F} is given in (72) in Appendix A.5. Next, starting from Definition 2, the l -th marginal eigenvalue pdf is derived as follows:

$$\begin{aligned} p_l(\lambda_l; m_1, m_2, q) &= \int_{\lambda_l}^{+\infty} \cdots \int_{\lambda_2}^{+\infty} \left[\int_0^{\lambda_l} \cdots \int_0^{\lambda_{q-1}} p_{\lambda}(\boldsymbol{\lambda}) d\lambda_q \cdots d\lambda_{l+1} \right] d\lambda_1 \cdots d\lambda_{l-1} \\ &\stackrel{(a)}{=} K_{p_l} \sum_{n_1=1}^q \sum_{n_2 \neq n_1=1}^q \cdots \sum_{n_l \neq n_1, \dots, n_{l-1}=1}^q \sum_{m_1=1}^q \sum_{m_2 \neq m_1=1}^q \cdots \sum_{m_l \neq m_1, \dots, m_{l-1}=1}^q s((n_1, \dots, n_l), (m_1, \dots, m_l)) \end{aligned}$$

$$\times \det(\Xi(l, m_1, m_2, q, \mathcal{I}^{[l, (n_1, \dots, n_l)]}, \mathcal{I}^{[l, (m_1, \dots, m_l)]})) \varphi(n_l, m_l, \lambda_l) \prod_{i=1}^{l-1} \int_{\lambda_i}^{+\infty} \varphi(n_i, m_i, \lambda) d\lambda, \quad (79)$$

where K_{p_l} is a constant ensuring that the integral over the pdf equals one, and (a) is obtained using [30, Eq. (50)], which can be used for computing the integral in (39). Based on (72), the function $\varphi(n, m, x)$ in [30, Eq. (50)] is written as $\varphi(n, m, x) = \phi_n(x)\psi_m(x)\xi(x)$, where $\phi_n(x) = x^{n-1}$, $\psi_m(x) = x^{m-1}$, and $\xi(x) = \frac{x^{m_2-q}}{(1+x)^{m_1+m_2}}$. Furthermore, the multiple summations in (79) can be equivalently reformulated in terms of the recurrence relation in (43). Lastly, special integrals are computed using the definition of the incomplete Beta function and the hypergeometric function from [36] to obtain the expressions in Theorem 4. \square

REFERENCES

- [1] A. Krishnamoorthy, R. Schober, and Z. Ding, "Downlink precoder design for two-user power-domain MIMO-NOMA with excess degrees of freedom," in *Proc. IEEE Int. Conf. Commun. Workshops*, May 2019, pp. 1–6.
- [2] A. Krishnamoorthy and R. Schober, "Statistical power allocation for downlink two-user power-domain MIMO-NOMA with excess degrees of freedom," *Proc. 24th Intl. ITG Workshop on Smart Antennas, Hamburg, Germany*, 2019.
- [3] Y. Saito, Y. Kishiyama, A. Benjebbour, T. Nakamura, A. Li, and K. Higuchi, "Non-orthogonal multiple access (NOMA) for cellular future radio access," in *Proc. IEEE 77th Veh. Technol. Conf.*, Jun. 2013, pp. 1–5.
- [4] Z. Ding, X. Lei, G. K. Karagiannidis, R. Schober, J. Yuan, and V. K. Bhargava, "A survey on non-orthogonal multiple access for 5G networks: Research challenges and future trends," *IEEE J. Sel. Areas Commun.*, vol. 35, no. 10, pp. 2181–2195, Oct. 2017.
- [5] S. M. R. Islam, N. Avazov, O. A. Dobre, and K. Kwak, "Power-domain non-orthogonal multiple access (NOMA) in 5G systems: Potentials and challenges," *IEEE Commun. Surveys & Tutorials*, vol. 19, no. 2, pp. 721–742, 2017.
- [6] L. Dai, B. Wang, Z. Ding, Z. Wang, S. Chen, and L. Hanzo, "A survey of non-orthogonal multiple access for 5G," *IEEE Commun. Surveys & Tutorials*, vol. 20, no. 3, pp. 2294–2323, 2018.
- [7] Z. Ding, Z. Yang, P. Fan, and H. V. Poor, "On the performance of non-orthogonal multiple access in 5G systems with randomly deployed users," vol. 21, pp. 1501–1505, 2014.
- [8] Y. Liu, G. Pan, H. Zhang, and M. Song, "On the capacity comparison between MIMO-NOMA and MIMO-OMA," *IEEE Access*, vol. 4, pp. 2123–2129, May 2016.
- [9] M. Zeng, A. Yadav, O. A. Dobre, G. I. Tsiropoulos, and H. V. Poor, "On the sum rate of MIMO-NOMA and MIMO-OMA systems," *IEEE Wireless Commun. Lett.*, vol. 6, no. 4, pp. 534–537, Aug. 2017.
- [10] Z. Ding, R. Schober, and H. V. Poor, "A general MIMO framework for NOMA downlink and uplink transmission based on signal alignment," *IEEE Trans. Wireless Commun.*, vol. 15, no. 6, pp. 4438–4454, Jun. 2016.
- [11] Z. Chen, Z. Ding, P. Xu, and X. Dai, "Optimal precoding for a QoS optimization problem in two-user MISO-NOMA downlink," *IEEE Commun. Lett.*, vol. 20, no. 6, pp. 1263–1266, Jun. 2016.
- [12] Z. Chen, Z. Ding, P. Xu, X. Dai, J. Xu, and D. W. K. Ng, "Comment on "optimal precoding for a QoS optimization problem in two-user MISO-NOMA downlink"," *IEEE Commun. Lett.*, vol. 21, no. 9, pp. 2109–2111, Sep. 2017.
- [13] S. Ali, E. Hossain, and D. I. Kim, "Non-orthogonal multiple access (NOMA) for downlink multiuser MIMO systems: User clustering, beamforming, and power allocation," *IEEE Access*, vol. 5, pp. 565–577, Dec. 2017.

- [14] M. Zeng, A. Yadav, O. A. Dobre, G. I. Tsiropoulos, and H. V. Poor, "Capacity comparison between MIMO-NOMA and MIMO-OMA with multiple users in a cluster," *IEEE J. Sel. Areas Commun.*, vol. 35, no. 10, pp. 2413–2424, Oct. 2017.
- [15] M. F. Hanif and Z. Ding, "Robust power allocation in MIMO-NOMA systems," *IEEE Wireless Commun. Lett.*, vol. 8, pp. 1541–1545, 2019.
- [16] P. Liu, Y. Li, W. Cheng, W. Zhang, and X. Gao, "Energy-efficient power allocation for millimeter wave beamspace MIMO-NOMA systems," *IEEE Access*, vol. 7, pp. 114 582–114 592, 2019.
- [17] B. Wang, R. Shi, C. Ji, and J. Hu, "Joint precoding and user scheduling for full-duplex cooperative MIMO-NOMA V2X networks," in *Proc. IEEE 90th Vehicular Technology Conf. (VTC2019-Fall)*, Sep. 2019, pp. 1–6.
- [18] Y. S. Xiao and D. H. K. Tsang, "Interference alignment beamforming and power allocation for cognitive MIMO-NOMA downlink networks," in *Proc. IEEE Wireless Commun. Netw. Conf. (WCNC)*, Apr. 2019, pp. 1–6.
- [19] W. Shao, S. Zhang, X. Zhang, J. Ma, and N. Zhao, "Suppressing interference and power allocation over the multi-cell MIMO-NOMA networks," *IEEE Commun. Lett.*, vol. 23, no. 8, pp. 1397–1400, Aug. 2019.
- [20] J. Ding, J. Cai, and C. Yi, "An improved coalition game approach for MIMO-NOMA clustering integrating beamforming and power allocation," *IEEE Trans. Veh. Technol.*, vol. 68, no. 2, pp. 1672–1687, Feb. 2019.
- [21] Z. Ma, Z. Ding, P. Fan, and S. Tang, "A general framework for MIMO uplink and downlink transmissions in 5G multiple access," in *Proc. IEEE 83rd Veh. Technol. Conf.*, May 2016, pp. 1–4.
- [22] Z. Chen, Z. Ding, X. Dai, and R. Schober, "Asymptotic performance analysis of GSVD-NOMA systems with a large-scale antenna array," *IEEE Trans. Wireless Commun.*, vol. 18, no. 1, pp. 575–590, Jan. 2019.
- [23] A. K. Gupta and D. K. Nagar, *Matrix Variate Distributions*. CRC Press, 1999, vol. 104.
- [24] A. Wiesel, Y. C. Eldar, and S. Shamai, "Zero-forcing precoding and generalized inverses," *IEEE Trans. Signal Process.*, vol. 56, no. 9, pp. 4409–4418, Sept 2008.
- [25] Q. H. Spencer, A. L. Swindlehurst, and M. Haardt, "Zero-forcing methods for downlink spatial multiplexing in multiuser MIMO channels," *IEEE Trans. Signal Process.*, vol. 52, no. 2, pp. 461–471, Feb. 2004.
- [26] C. F. Van Loan, "Generalizing the singular value decomposition," *SIAM Journal on Numerical Analysis*, vol. 13, no. 1, pp. 76–83, Mar. 1976.
- [27] C. C. Paige and M. A. Saunders, "Towards a generalized singular value decomposition," *SIAM Journal on Numerical Analysis*, vol. 18, no. 3, pp. 398–405, Jul. 1981.
- [28] Z. Bai, "The CSD, GSVD, their applications and computations," *Preprint Series 958, Institute for Mathematics and its Applications, University of Minnesota*, 1992.
- [29] C. Van Loan, "Computing the CS and the generalized singular value decompositions," *Numerische Mathematik*, vol. 46, no. 4, pp. 479–491, Dec. 1985.
- [30] A. Zanella, M. Chiani, and M. Z. Win, "On the marginal distribution of the eigenvalues of Wishart matrices," *IEEE Trans. Commun.*, vol. 57, no. 4, Apr. 2009.
- [31] M. D. Perlman, "A note on the matrix-variate F distribution," *Sankhyā: The Indian Journal of Statistics, Series A*, pp. 290–298, Jul. 1977.
- [32] P. J. Forrester, "Eigenvalue statistics for product complex Wishart matrices," *Journal of Physics A: Mathematical and Theoretical*, vol. 47, no. 34, p. 345202, Aug. 2014.
- [33] Z. Chen, Z. Ding, and X. Dai, "On the distribution of the squared generalized singular values and its applications," *IEEE Trans. Veh. Technol.*, vol. 68, no. 1, pp. 1030–1034, Jan. 2019.
- [34] A. M. Tulino, S. Verdú *et al.*, "Random matrix theory and wireless communications," *Foundations and Trends in Communications and Information Theory*, vol. 1, no. 1, pp. 1–182, 2004.

- [35] A. Zanella and M. Chiani, "The PDF of the l th largest eigenvalue of central wishart matrices and its application to the performance analysis of MIMO systems," in *Proc. IEEE Global Telecommun. Conf.*, Nov. 2008, pp. 1–6.
- [36] F. W. Olver, D. Lozier, R. Boisvert, and C. Clark, "NIST digital library of mathematical functions," *Release*, vol. 1, p. 14, 2010. [Online]. Available: <https://dlmf.nist.gov/>.
- [37] X. Wang and G. B. Giannakis, "Resource allocation for wireless multiuser OFDM networks," *IEEE Trans. Inf. Theory*, vol. 57, no. 7, pp. 4359–4372, 2011.
- [38] A. L. Yuille and A. Rangarajan, "The concave-convex procedure," *Neural computation*, vol. 15, no. 4, pp. 915–936, 2003.
- [39] T. Lipp and S. Boyd, "Variations and extension of the convex–concave procedure," *Optimization and Engineering*, vol. 17, no. 2, pp. 263–287, 2016.
- [40] D. K. Nagar and A. K. Gupta, "Expectations of functions of complex Wishart matrix," *Acta Applicandae Mathematicae*, vol. 113, no. 3, pp. 265–288, Mar. 2011.
- [41] P. J. Forrester, *Log-gases and random matrices (LMS-34)*. Princeton University Press, 2010.